The miR-96/RARγ signaling axis governs androgen signaling and prostate cancer progression

Mark D Long[1], Prashant K Singh[2], James R Russell[1], Gerard Llimos[1a],

Spencer Rosario[1], Abbas Rizvi[3], Patrick R. van den Berg[1b], Jason Kirk[4],

Lara E Sucheston-Campbell[3,5], Dominic J Smiraglia[1], Moray J Campbell[6]

[1]Department of Cancer Genetics and Genomics, Roswell Park Cancer Institute, Buffalo, NY, 14263, USA

[2]Genomics Core Facility, Roswell Park Cancer Institute, Buffalo, NY, 14263, USA

[3]College of Pharmacy, The Ohio State University, Columbus, OH 43210

[4]Department of Pharmacology & Therapeutics, Roswell Park Cancer Institute, Buffalo, NY, 14263, USA

[5]College of Veterinary Medicine, The Ohio State University, Columbus, OH 43210

[6]Division of Pharmaceutics and Pharmaceutical Chemistry, College of Pharmacy, 536 Parks Hall, The Ohio State University, Columbus, OH 43210

[a]Current address Institute of Bioengineering, École Polytechnique Fédérale de Lausanne (EPFL), Lausanne, Switzerland.

[b]Current address: Leiden institute of Physics, Leiden University, 2300 RA Leiden, Netherlands

Running title: RARγ and prostate cancer

Conflict of interest: The authors certify that they have NO affiliations with or involvement in any organization or entity with any financial interest (such as honoraria; educational grants; participation in speakers' bureaus; membership, employment, consultancies, stock ownership, or other equity interest; and expert testimony or patent-licensing arrangements), or non-financial interest (such as personal or professional relationships, affiliations, knowledge or beliefs) in the subject matter or materials discussed in this manuscript.

ABSTRACT

RARγ (*RARG*) expression is commonly reduced in prostate cancer (PCa). Modulating RARγ levels, not retinoid ligand, had the biggest impact on prostate cell proliferation and gene expression. Genomic binding of the non-liganded, *apo,* RARγ was significantly enriched at active enhancers, associated with AR, and RARγ knockdown governed the AR capacity to regulate cell differentiation and gene-regulation. Altered RARγ target genes expression in TCGA significantly associated with more aggressive PCa. RARγ downregulation was explained by a stark and common increase in miR-96 in PCa cell and animal models, and human PCa. Biochemical approaches confirmed that miR-96 directly regulates *RARG* expression and function. Capture of the miR-96 targetome by biotin-miRNA pulldown identified a RARγ-centric network significantly associated with more aggressive PCa and worse disease free survival (hazard ratio 2.23, 95% CI 1.58 to 2.88, p=0.015). In summary, miR-96 targets an RARγ network to govern AR signaling and its disruption is a cancer-driver.

STATEMENT OF SIGNIFICANCE.

We identified that miR-96 targets a RARγ-network, which in turn regulates AR, PCa progression and disease outcome. These findings occur independently of retinoid ligand and reveal how miRNA govern nuclear receptor functions, and can be exploited to identify aggressive prostate cancer at an early stage.

INTRODUCTION

Members of the nuclear hormone receptor (NR) superfamily are ubiquitously expressed across tissues and govern cell fate decisions. One NR, the androgen receptor (*AR/NR3C4*), is a key regulator of growth and differentiation in the prostate gland(1). Genomic approaches in prostate cancer (PCa) have identified that the capacity of the AR becomes skewed with disease progression(2). A normal component of AR signaling is to drive terminal differentiation of luminal epithelial cells and the phenotypic consequences of altering AR signaling capacity is, in part, to disrupt this function(3). The disruption, or re-wiring, of AR action changes both the receptor sensitivity, defined as the magnitude of the transcriptional response, and capacity, defined as the selection of gene networks governed. Although the AR is a pharmacological target in later PCa stages, its disruption at early stage disease is more nuanced(4).

In fact, multiple NRs are expressed in the normal prostate and are disrupted in PCa. NR actions are integrated by shared genomic binding regions, shared co-factors and the co-regulation of ligand availability(5,6). Non-coding RNAs, including miRNA and lncRNA target NRs, their co-factors and target genes to also exert control of signaling (7,8). Combined, these different aspects of NR regulation generate sensitivity.

As a route to identify how NR networks are disrupted in cancer we undertook a pan-cancer analysis of the NR superfamily in The Cancer Genome Atlas (TCGA). Significantly distinct NR profiles were revealed within each tumor type (9,10). Specifically, in the Taylor et al MSKCC(11) and TCGA-PRAD PCa cohorts(12) the retinoic acid receptor gamma (*NR1B3*/*RARG*, encodes RARγ) and glucocorticoid receptor (*NR3C1/GR*) were significantly and uniquely down-regulated. By contrast, the AR was not significantly altered in either cohort. There was only one *RARG* mutation and relatively few CNVs detected at the *RARG* locus across these approximately 600 PCa samples.

To better understand the consequences and causes of reduced RARγ in prostate cells we inspected the impact of reduced RARγ expression on cell phenotypes and gene expression, in the *apo* (non-ligand stimulated) and *holo* (ligand-stimulated) states, and found a substantial regulatory function specific to the *apo*-RARγ condition. Combined with analyses of the RARγ cistrome, these findings revealed that *apo*-RARγ significantly associates with active gene enhancers, and impacts other transcription factor functions, including those of the AR. Testing how the RARγ governed the capacity and sensitivity of AR was undertaken by androgen-dependent transcriptomic analyses in cells with altered RARγ expression.

Furthermore we revealed that miRNA-96 regulates expression of RARγ and several known RARγ co-factors, and that miR-96 is commonly elevated in PCa associated with disease progression. Finally, across multiple PCa cohorts the miR-96 targetome and RARγ-dependent transcriptome associated with aggressive PCa and disease progression.

Together these findings support several innovative concepts. Firstly, that miR-96 potently regulates RARγ because it co-targets a number of RARγ-interacting co-factors. Secondly, the major gene regulatory (and disease associated) functions of RARγ are largely independent of retinoid activation. Thirdly, regulation of this RARγ network is a potent disease driver because it is a major regulator of AR sensitivity and capacity.

RESULTS

Reduced RARγ expression promotes cell proliferation and widely alters gene expression in non-malignant and malignant prostate cell models.

To test if reduced RARγ levels are pro-tumorigenic, and to what extent retinoid responses are RARγ dependent, we knocked-down RARγ levels in non-malignant prostate epithelial cells (RWPE1) and LNCaP PCa cells using two separate RARγ targeting shRNA constructs (**Supplementary Figure 1A-F**). In RWPE1 and LNCaP cells in standard cell tissue culture conditions and without exogenous retinoids, RARγ knockdown increased growth rates within 72 hr (**Figure 1A**). By contrast, RARγ knockdown only modestly reduced anti-proliferative sensitivity in RWPE1 to either all-trans retinoic acid (ATRA) or RARγ-selective ligand, CD437 (**Supplementary Figure 2A-D**). Also, independent of exposure to ligand, RARγ knockdown significantly reduced the G_2/M population in both RWPE1 and LNCaP cells, whereas only in RWPE1 cells, reduced RARγ levels changed CD437-induced G_2/M blockade (**Supplementary Figure 2E-F**). Together these findings suggest that reducing RARγ expression has profound biological effects on growth and cell cycle control, which is largely independent of exogenous ligand.

Reducing RARγ levels exerted a significant impact on gene expression in the absence of ligand stimulation (*apo* function). The RARγ dependent CD437-induced response (*holo* function), defined as genes differentially regulated by CD437 in shCTL cells but not (or to a significantly lesser extent) in shRARG cells, was more modest (RWPE1) or negligible (LNCaP) (**Figure 1B-C**, **Supplementary Figure 3**). In RWPE1 cells, 605 differentially expressed genes (DEGs) (1.2 fold change, Benjamini-Hochberg adjusted p-value < 0.05) were associated with *apo* RARγ regulation, whereas only 237 genes were responsive to CD437 (10 nM, 24 hr) in a RARγ dependent manner. In both cases the proportion of up-regulated genes was significantly higher. For example, proportionately more genes were up- (N=338 gene) than down-regulated (N=265) for the *apo*-transcriptome (p<0.001).

To infer functionality, Gene Set Enrichment Analysis (GSEA) was applied to the *apo* and *holo* RARγ dependent transcriptomes. 435 pathways were enriched (normalized enrichment score (NES) > 1.8, FDR q-val < 0.05) in at least one comparison (**Supplementary Figure 3F**). Amongst these, 196 were associated uniquely with *apo* function and 201 with *holo*, while 38 were common between categories. Frequency mining of common terms combined with hypergeometric testing established largely distinct enrichment of meta-groups (e.g. terms

associated with NF-κB) between the *apo* and *holo* RARγ states in both RWPE1 and LNCaP cells (**Figure 1D**). In RWPE1 cells *apo* transcriptome was significantly enriched for terms associated with NF-κB and histone deacetylase (HDAC) function (**Figure 1E**) whereas the *holo* transcriptome was enriched for terms related to Tretinoin (the commercial name for ATRA) (**Figure 1F**), as well as for ESR function. In LNCaP cells the *apo* RARγ gene regulatory effects were most pronounced (**Supplementary Figure 3C-D**) and highly enriched for hypoxia and AR responses (**Figure 1G, Supplementary Figure 3E-F**).

Reflecting the enrichment of AR terms in the apo transcriptome in LNCaP, we used a previously compiled AR target gene panel (12) to demonstrate that expression of these genes alone significantly distinguished LNCaP-shRARG cells from controls, in a CD437-independent manner (**Figure 1H**). Furthermore, knockdown of RARγ in LNCaP also altered the DHT-induced expression changes in several key androgen target genes (i.e. *KLK3*, *TMPRSS2*) (**Supplementary Figure 3H**).

In total, these findings indicate that *apo* RARγ function is substantial and intertwined with other transcription factors, notably the AR and NF-κB, and functionally-independent of the *holo* RARγ.

The *apo* RARγ cistrome significantly overlaps with active enhancers, AR cistromes and associates with aggressive PCa.

Next, we measured the *apo* and *holo* RARγ cistromes using RARγ-EGFP stably transfected in RWPE1 cells (13); optimization studies confirmed modestly-elevated RARγ-EGFP levels compared to endogenous RARγ, and enrichment at RARγ dependent genes (**Supplementary Figure 4A-C**). Reflecting the transcriptomic data, the *apo* RARγ cistrome was considerably larger (1256 peaks (p.adj < 0.1)) than the CD437-dependent cistrome of 360 peaks, of which 316 were shared, 44 were unique. Motif analyses of the *apo* RARγ cistrome revealed significant enrichment of transcription factor (TF) motifs for members of the AP1 family (FOSB/JUN), the homebox family (OTX2, PITX1) and NRs (RXRs, RARs). By contrast, and *holo* RARγ cistrome was enriched uniquely for CPEB1, ONEC2, HIC2 motifs as well as for FOSB/JUN (**Table 1**).

To characterize the RARγ cistrome further, we examined its genomic distribution and genomic overlaps, within 100bp, with publically available RWPE1 data, namely DNAse sensitivity, histone modifications (H3K27ac, H3K27me3, H3K4me1, H3K4me3) (GSE63094, GSM1541008), and the chromatin states track derived with ChromHMM (14). Alongside these,

we also examined normal prostate epithelial cell enhancers (15) and AR, ERα and NF-κB-dependent cistromes derived in PCa cells (2) (**Figure 2A,B,C**).

A clear and significant overlap between the *apo* RARγ cistrome with H3K27ac, H3K4me1 and was identified associated with enhancer status (**Figure 2A, upper**) and TSS of expressed target genes (**Figure 2A, lower**); specifically, 829 RARγ binding sites overlapped with combined H3K27ac, H3K4me1 and DNAse sensitivity profiles suggesting that the *apo* RARγ is commonly found in open chromatin active enhancer regions (**Figure 2B**). Reflecting the transcriptome data of RARγ function overlapping with AR and NF-κB functions (**Figure 1D**), significant overlaps were also identified between RARγ binding and both the *apo* and *holo* AR(16), and the DHT-dependent and TNF-stimulated p65 cistrome (2) (**Figure 2C**). This was also supported by the ChromHMM track showing binding of RARγ at sites of poised and flanking transcription (e.g. **Figure 2D**).

Next, we sought to dissect transcriptome-cistrome relationships. Candidate level-relationships were identified. *Apo* RARγ binds at the KRT15 locus in active enhancer sites, and its transcription is significantly altered by the knockdown of RARγ (**Figure 2D, E**). To test the genome-wide level of significance transcriptome-cistrome relationships both *apo* and *holo* RARγ cistromes were annotated to within 7.5 kb of known gene TSS. The mean expression of these cistrome proximal genes were then compared with that of genes found to be RARγ dependent from expression studies using a random sampling with replacement, or bootstrapping, approach (**Supplementary Table 1**). *Apo* and *holo* RARγ cistromes were significantly associated with genes whose expression changed upon loss of RARγ, supporting a functional relationship between RARγ binding and expression control (**Figure 2F**).

In the TCGA-PRAD and MSKCC cohorts the RARγ-annotated genes significantly positively correlated with RARγ **(Supplementary Figure 5A,B)** filtering these RARγ cistrome genes (altered by greater than 2 Z-scores in more 35% tumors relative to normal tissue) identified 58 genes. Expression of these genes stratified patients (**Figure 2G**) and distinguished a cluster of high Gleason grade tumors (adjusting for age) (p-value = 0.038). We also reasoned that higher Gleason grade tumors were associated with worse outcome and therefore we tested relationships between the expression of individual genes and disease free survival. After FDR correction, four of these genes were individually significantly associated with disease free survival; the steroidogenic enzyme *CYP11A* (**Figure 2H**); *LRG6*, a WNT regulator and implicated in breast cancer; *PRR7*, a central regulator of CLOCK;.

Reduced RARγ expression alters AR signaling capacity and sensitivity.

The cellular phenotype, transcriptome and cistrome data support the concept that *apo* RARγ actions are a substantial portion of all RARγ genomic functions and intertwined with other TFs including the AR. Therefore, we sought to test the genome-wide impact of RARγ expression on AR function directly in non-malignant prostate epithelial HPr1AR cells. These cells constitutively express AR, and undergo androgen-induced differentiation from a basal-like towards a more luminal-like phenotype (17). RARγ knockdown reduced RARγ levels 60-80%, which was not altered by DHT (**Supplementary Figure 6A-D**).

The anti-proliferative response induced by DHT was significantly dampened in RARγ knockdown HPr1AR cells (**Figure 3A**). We therefore investigated whether the *apo* RARγ functions to govern AR signaling capacity and/or sensitivity. At the transcriptome level (RNA-Seq), RARγ knockdown substantially reduced DHT-dependent transcriptome changes at both 24 and 96 hr (**Figure 3B-C, Supplementary Figure 7A-B**). At 24 hr, 1454 of the 2309 (63.0%) DHT-regulated DEGs were either no longer regulated or had significantly dampened regulation in RARγ knockdown HPr1AR cells. The sensitivity switch in response to RARγ loss was directional, as all DHT-responses were dampened rather than amplified. However, the capacity of DHT regulation was also shifted, albeit to a lesser extent, as a small number of genes (109) gained unique DHT-regulation following RARγ knockdown in HPr1AR cells at 24 hr. Thus, RARγ knockdown substantially impacted both the sensitivity and the capacity of the AR-regulated transcriptome.

GSEA identified enrichment for androgen response (**Figure 3D-F**), MYC and hypoxia associated pathways (17); these pathways are consistent with a shift towards luminal differentiation and an anti-proliferative response to DHT. Indeed, the extent of AR pathway regulation by DHT was significantly reduced in RARγ knockdown HPr1AR cells. For example, classic androgen response pathways were not elevated to the same extent in RARγ knockdown cells relative to parental HPr-1AR cells, and conversely the repression of MYC regulated pathways was less apparent. Notably, a prominent RARγ binding peak was identified in an enhancer region upstream of MYC (**Supplementary Figure 7D**).

Together, this suggest that RARγ expression governs AR function in normal prostate cells independently of exogenous retinoid ligand, and that RARγ loss dampens both phenotypic and transcriptomic androgen responses, which manifest as reduced luminal differentiation and reduced antiproliferative signaling.

Elevated miR-96 drives reduced RARγ expression and associates with aggressive prostate cancer.

The frequent downregulation of *RARG* reflected neither mutation nor copy number variation(10) and therefore we considered epigenetic mechanisms, but found no evidence for altered DNA methylation in the TCGA-PRAD cohort (**Supplementary Figure 8**). Therefore, we considered miRNA, and used *in silico* prediction tools(18) to define a cohort of miRNAs that target the most common previously identified downregulated NRs (i.e. *RARG, GR*) in the TCGA-PRAD and MSKCC cohorts (10).

Specifically, 61 putative NR-targeting miRNAs were identified (**Supplementary Figure 9**) which are collectively significantly elevated in PCa samples (p.adj = 0.02) and are reciprocal to the reduction of NR mRNA expression. The miR-96-182-183 cluster was amongst the most commonly upregulated miRNAs. Although similar, base substitutions in the targeting regions of each miRNA suggest unique functionality (**Supplementary Figure 10A**). Only miR-96 and miR-182 have predicted target sequences in the *RARG* 3'UTR (**Supplementary Figure 10B**).

In both the MSKCC and PRAD cohorts, *RARG* significantly and negatively correlated with cluster members, but most strongly with miR-96 (**Figure 4A**). Expression analyses in a panel of prostate cell lines (**Figure 4B**) revealed miR-96 increases relative to non-malignant RWPE1 and HPr1AR cells, in six PCa cell lines and reduction in *RARG* expression. Profiling in PCa mouse models revealed reduced *Rarg* in both Pten$^{-/-}$(19) and to a greater extent in TRAMP but, interestingly, not in Hi-MYC mice (**Supplementary Figure 11A**). *Rarg* expression decreased dynamically with PCa development in TRAMP mice, relative to age-matched wild-type controls (C57BL/6), and inversely correlated most significantly with elevated miR-96 expression (Pearson's r = -0.88) (**Figure 4C**, **Supplementary Figure 11B**). Notably, significant expression changes were observed as early as 10 weeks of age, when TRAMP mice display prostate epithelial hyperplasia. Finally, the negative correlation of *RARG* and miR-96 cluster members were validated in an independent cohort of 36 matching tumor/normal prostate tissue pairs, and significantly associated with Gleason sum (**Supplementary Figure 12A-C**), corroborating observations in TCGA-PRAD and MSKCC cohorts. Additionally miR-96 expression in the TCGA-PRAD cohort stratified patients based on shorter disease free survival (**Supplementary Figure 12D**). Together these findings in murine and human prostate tissues suggest that increased miR-96 expression occurs early, and is sustained in PCa development, correlates strongly with loss of *RARG* and associates with aggressive PCa outcomes.

Two miR-96 recognition elements were identified in the *RARG* 3'UTR region (**Supplementary Figure 10B**). Ectopic overexpression of miR-96 resulted in significant loss of RARγ mRNA and protein in both RWPE1 and LNCaP cells (**Figure 4D, Supplementary Figure 13A-C**) and co-transfection of a *RARG* 3'UTR luciferase vector with a miR-96 mimic resulted in significant loss of luciferase activity (**Figure 4E**). Finally, miR-96 suppressed RARγ ligand-dependent induction and repression of target genes, which was alleviated by a miR-96 antagomiR (**Figure 4F**).

Lastly, transfection with miR-96 mimics led to a marked increase of proliferation in LNCaP cells, reflecting phenotypes observed in RARγ knockdown cells (**Figure 1**). Exogenous miR-96 also altered the cell-cycle distribution. In LNCaP cells there was a loss of cells in G_1/G_0 phase (53.2% relative to 64.8%) and increase in S and G_2/M phase (**Figure 4G** and **Supplementary Figure 14**). However, cell cycle shifts in LNCaP did not mirror those observed in RARγ knockdown cells, and no significant changes were noted in RWPE1 cells, suggesting that miR-96 related phenotypes involve additional targets other than RARγ.

Together, these findings support the concept that elevated miR-96 targets and suppresses *RARG* expression and function, an interaction which occurs early in PCa progression and which has pro-tumorigenic properties.

MiR-96 targets a network of RARγ interacting co-factors.

While these data strongly support miR-96 targeting of RARγ, other studies have identified additional targets, including the pioneer factor FOXO1(20), which have biological consequence in prostate cells. Therefore, to reveal all miR-96 targets (the miR-96 targetome), we undertook a biotin-miRNA (bi-miR) pulldown approach coupled with microarray analyses(21). Biotin labelling of miR-96 mimics did not interfere with either transfection or knockdown of target gene expression (**Supplementary Figure 15A-B**), and was able to capture known (e.g. *RARG* and *FOXO1*) and predicted (*TBL1X*) miR-96 targets (**Supplementary Figure 15C**). PCA revealed strong separation of experimental groups (**Supplementary Figure 15D**).

The bi-miR-96 pulldown revealed 111 and 389 miR-96 targets in RWPE1 and LNCaP cells, respectively, which were largely shared, but also had unique genes (**Figure 5A-B Supplementary Figure 15E**). Amongst these targets, 3'UTR miR-96 target site motifs (GTGCCAA) was the most highly enriched (**Figure 5C**) (GSEA in LNCaP p.adj = $1.24e10^{-26}$, RWPE1 p.adj = $1.70e10^{-9}$). RT-qPCR validation of independent LNCaP cells confirmed the direct binding of miR-96 to known and novel targets identified from profiling (**Supplementary Figure 15F**).

Interestingly, in LNCaP cells *FOXO1* was neither significantly enriched in the bi-miR-96 fraction upon microarray analysis and was only validated by RT-qPCR in RWPE1 cells. Also surprisingly, *RARG* transcript was not significantly detectable via microarray in either LNCaP or RWPE1 cells, but did validate by RT-qPCR in both cell types. It was revealed that the Illumina HT12v4 Bead Chip array contains only a single exon probe targeting a single *RARG* isoform. *RARG* expression in LNCaP cells has been reported (22) suggesting that the microarray finding is a false negative one.

The capacity of miR-96 to suppress target gene expression was also assessed by independent transfections of biotinylated and non-biotinylated miR-96 mimics. In LNCaP cells, 6 out of 7 bi-miR-96 identified targets were significantly downregulated by both miR-96 and bi-miR-96 relative to respective non-targeting controls, while a negative control target *CDH1* was not affected (**Figure 5D**). Intriguingly, the single transcript not downregulated in this experiment, p27 (encoded by *CDKN1B*), showed significantly reduced protein level upon miR-96 overexpression, suggesting that in some cases the result of miR-96 binding is translational inhibition not degradation of transcript (**Supplementary Figure 15G, H**).

Functional annotation of the miR-96 targetome in LNCaP cells based on GO terms revealed roles for miR-96 in governing cell cycle progression, metabolism, cell morphology and microtubule organization (**Supplementary Figure 16A,B**). These observations reflected the impact of miR-96 on cell cycle and included *CDKN1B*, *CDK2*, *DICER1* and transforming acidic coiled-coil protein 1 (*TACC1*). The top five most significant inverse miR-96/mRNA relationships included cell-cycle regulators and transcription factors. Expression after miR-96 overexpression in LNCaP cells revealed several were significantly suppressed (**Supplementary Figure 16C,D**).

To assess whether experimentally determined targets had relationships in clinical samples, TCGA-PRAD data were again examined. Genes within the miR-96 targetome showed a significantly more negative correlation with miR-96 expression than the background transcriptome, supporting a functional relationship ($p = 5.17e^{-7}$) (**Figure 5E**). Stringent filtering of expression of the miR-96 targetome genes (+/-2 Z scores in 35% of tumors relative to normal prostate tissue) identified 22 altered genes segregated invasive tumors (Pathological N1), after adjusting for age at diagnosis (p-value = 0.041) (**Figure 5F**). Five of these 22 genes were known to regulate RAR signaling (i.e. *TACC1*(23), *ZIC2*(24), *PRKAR1A*(25), *EIF4G2*(26), and others were such are *ONECUT2* are putative co-regulator (27). Interestingly, the motif for ONCUT2 was enriched in the experimentally derived *holo* RARγ cistrome.

The miR-96 governed RARγ network drives aggressive prostate cancer.

Several lines of evidence support the concept that miR-96/RARγ is a significant signaling axis in the prostate; the levels alone of *apo* RARγ control gene expression and govern AR function; miR-96 governs the levels of *apo* RARγ and a number of interacting co-factors; the expression of miR-96 and RARγ are reciprocal in murine and human tumors; RARγ targets and miR-96 targets predict aggressive PCa tumors.

Of the RARγ-network genes, TACC1 had the strongest positive correlation with RARγ, and only the cross-correlations with either RARγ or TACC1 to RARγ target genes were significantly different between tumors expressing high or low levels of miR-96 (**Supplementary Figure 17**). Therefore we sought to establish the combined significance of miR-96/RARγ axis in PCa by segregating tumors in the TCGA-PRAD cohort into low expression of RARγ and TACC1, and high miR-96 expression. These were compared to the reciprocal (high RARγ and TACC1, low miR-96) (**Figure 6A**). Differential expression identified ~1700 genes, which were in turn overlapped with the gene sets developed through the study. Several of the overlaps support the concept of a miR-96/RARγ axis. Nearly 200 genes were shared between the *apo* RARγ-dependent gene expression and the DHT-regulated and shRNA RARγ-dependent genes, and 31 of these significantly overlapped (p=7.1e-6) with the genes identified in TCGA-PRAD (**Figure 6A**).

We reasoned that if genes central to the miR-96/RARγ axis were critical in PCa, they would be commonly distorted and associate with aggressive disease. Filtering the ~1700 differentially expressed genes in RARγ low/miR-96 high tumors (altered by +/-2 Z scores in more than 45% of tumors relative to normal prostate tissue) revealed 47 genes. These genes clustered tumors separated that significantly associated with worse disease free survival (X_REFS_IND) in the TCGA-PRAD cohort (hazard ratio 2.23, 95% CI 1.58 to 2.88, p=0.015), and also clustered high Gleason score tumors (p-val = 0.012) (**Figure 6B**). Genes were also annotated for whether they were an *apo* RARγ cistrome gene; DHT-regulated RARγ-dependent genes; and member of the highest rank GSEA term (LIU_PROSTATE_CANCER_DN; a cohort of genes significantly down-regulated in PCa(28)). Five RARγ cistrome genes were all down-regulated, including the tumor suppressor *MCC*(29) and other regulators of cell-fate such as *GPX3*(30) and *SOX15*(31) and furthermore *MCC* and *SOX15* were also DHT-regulated RARγ-dependent genes (**Figure 6C**). These findings support the concept that the miR-96/RARγ axis can be detected in PCa cohorts and underscores both its cross talk with AR signaling and its clinical relevance.

DISCUSSION

Developmental roles for RARγ have been identified in skin, skeletal and reproductive systems, including the prostate (32). Prostate epithelial squamous metaplasia arises in *Rarg-/-* mice, due to improper glandular function (32). More broadly, RARγ has emerged as an important transcription factor. For example, the Roadmap Epigenome consortium identified RARγ as a member of the most highly enriched in transcription factor-enhancer interactions across the human epigenome(33) and others have considered a role for the receptor to govern pluripotency(34). *RARG* has also been suggested to be a tumor suppressor in keratinocytes(35). Previously, we identified a common RARγ down-regulation in the TCGA-PRAD and MSKCC cohorts.

We have now identified that the *apo* actions of RARγ are substantial, and more significant than the impact of retinoid exposure, as seen with our microarray and ChIP studies, but also our analyses of microarray studies in RAR$\gamma^{-/-}$ murine ES cells and also F9 cells, (36) where similar patterns were observed (**Supplementary Figure 18**). These findings are also compatible with other receptors such as RARβ being more prominent in the sensing of exogenous ligand in PCa cells (37).

The current study also revealed RARγ regulation of AR signaling in PCa. The *apo* RARγ transcriptomic studies revealed enrichment of AR signaling processes, notably in LNCaP, whereas in RWPE1 cells the transcriptome was enriched for ESR function, further supporting RARγ functional crosstalk with steroid receptor signaling. Links between RARs and ER signaling which are well established in breast cancer(13).

Genomic *apo* RARγ binding very significantly overlapped with active enhancers (RWPE-1) and AR binding (LNCaP), and also significantly regulated the DHT-AR transcriptome in HPr-1AR cells. RARγ loss profoundly altered AR regulated events including DHT-mediated anti-proliferative effects (17) and reduced the DHT-dependent transcriptome, notably by restricting the capacity of AR to repress MYC signaling. Recently MYC has been shown to antagonize AR function in prostate cells(38), and the current study suggest that RARγ regulates these events, in part through direct binding at the MYC locus. Together these findings supported the concepts that the *apo* RARγ is significantly associated with enhancers, and governing AR functions.

Although miR-34c targets *RARG* in embryonic stem cells(39), we found no significant relationship between miR-34c and RARγ in the current study. Rather we identified miR-96, which has been investigated in various cancer settings including in PCa, but not associated with

RARγ (20,40). Furthermore, miR-96 is one of the 60 miRNAs whose expression most differentiated PCa clinical groups in TCGA-PRAD cohort. The current study extends these reports of oncogenic actions of miR-96 to identify the RARγ network as a major biological and clinically-relevant target.

The inverse relationships between miR-96 and RARγ was robust and significant across cell models, murine PCa models and clinical cohorts, and equal or greater than with previously identified targets including *FOXO1*. Biochemical tests established that miR-96 binds directly to multiple target sites contained within the 3'UTR of *RARG* and using the bi-miR approach revealed ~400 direct targets enriched for predicted miR-96 target sequences, and identified targets were directly bound and downregulated upon miR-96 overexpression.

Experimental over-expression of miR-96 positively regulated proliferation and cell cycle in PCa cells reflecting previous reports(20), but did not affect proliferation in non-malignant prostate cells. It is thus interesting to speculate that miR-96 acquires additional targets and subsequent functions within the malignant transcriptome, which coincides with the observation of 3-fold additional targets in malignant LNCaP cells relative to non-malignant RWPE1, and impacts the control of cell cycle progression. Given that RARγ appears to function as an important AR co-regulator to promote differentiation, then its downregulation by miR-96 targeting suggests an oncogenic action that shifts the AR signaling capacity in localized PCa. Notably, miR-96 has previously been reported as androgen regulated in prostate cells(41). Filtering miR-96 target genes to those most altered in PCa revealed that nearly one third (7/22) were within an RARγ-centric network of co-regulators, suggesting its regulation as an important aspect of miR-96 function.

Differential expression analyses in TCGA-PRAD cohort between tumors showing reciprocal expression of miR-96 and RARγ/TACC1 clustered aggressive tumors and predicted worse disease free patient survival. Several of these genes are either under-explored in PCa (i.e. SOX15 and MCC) or have only been investigated in metastatic PCa(42) (PPARGC1A). Together these date strongly support the concept that the miR-96/RARγ is a significant and yet under-explored regulator of the AR and drives PCa progression.

METHODS

Data analyses and integration

All analyses, were undertaken using the R platform for statistical computing (version 3.1.0) (43) (43) and a range of library packages were implemented in Bioconductor(44).

Cell culture and materials.

All cells were maintained in standard conditions in media recommended by ATCC. 2µg/mL puromycin was used for selection of pGIPz-shRARG and BAC-RARG-EGFP containing cell lines.

Cell proliferation and cell cycle analyses.

Bioluminescent detection of cellular ATP (proliferation) and cell-cycle distribution was determined utilizing FACSCalibur™ Flow Cytometer (Becton-Dickinson) and software.(8)

RT-qPCR.

Quantitative real-time reverse transcription–polymerase chain reaction (RT-qPCR) undertaken via Applied Biosystems 7300 Real-Time PCR System (Applied Biosystems), for both TaqMan® and SYBR® Green (SYBR® Green PCR Master Mix (Thermo Fisher Scientific)) applications(8). Fold changes were determined using the $2^{-\Delta\Delta Ct}$ method. Significance of experimental comparisons was performed using Student's t-test.

Western Immunoblotting

Western blot analysis of protein expression was undertaken as described previously . Membranes were probed with primary antibody against RARγ (sc550, Santa Cruz), GFP (ab290, Abcam or 2555S, Cell Signaling), or p27 (D37H1, Cell Signaling), either overnight at 4°C or for 3 hr at room temperature.

Expression determination in PCa mouse models

Snap frozen tissue and/or RNA from previously harvested normal or malignant prostate tissues of Hi-MYC, PTEN-/- and TRAMP (6, 8, 10, 15, 20-25 week) models, as well as from age-matched wild type (FVB:BL6, C57BL/6) mice, was obtained from the lab of Dr. Barbara Foster at RPCI. Relative expression of *Rarg* and microRNAs was determined in these tissues by RT-qPCR after normalization to *Gusb* or RNU6B, respectively.

miRNA mimic, antagomiR and siRNA transfection

Ectopic overexpression of miRNA was achieved by transient transfection of mirVana® miRNA mimics (30nM) (Ambion). Inhibition of miRNA was achieved by transient transfection of Anti-miR™ miRNA Inhibitor (30nM) (Ambion). For transient silencing of targets, siRNA was employed using Silencer® predesigned siRNAs (30nM) (Ambion). Transfection was accomplished by use of Lipofectamine® 2000 or Lipofectamine® 3000 by manufacturer's instructions. Concentrations of miRNA mimics and transfection reagents were optimized using BLOCK-iT™ Alexa Fluor® Red Fluorescent Control (Ambion) as well as by subsequent miRNA specific RT-qPCR and RT-qPCR of target mRNAs to assess efficiency of transfections.

RPCI PCa samples

RNA was obtained from a cohort of 36 men who underwent radical prostatectomy at RPCI and de-identified tissue made available through the Pathology Resource Network (PRN) and Data Bank and BioRepository (DBBR) shared resources at RPCI. Areas of histologically normal tissue and areas with high percentages of neoplastic tissue were isolated and RNA extracted. De-identified patient codes were matched with Gleason scores for each sample, were made available through the RPCI Clinical Data Network (CDN).

Molecular Cloning / Luciferase Assay

Luciferase assay was employed to assess direct targeting of miR-96 to the full length (FL) RARG 3'UTR or individual predicted target sites (t1, t2) within the RARG 3'UTR. RSV-pGL3-basic firefly luciferase expressing vector (Addgene) was employed for this purpose, utilizing FseI and XbaI restriction sites located between the *luc*+ gene and the SV40 pA tail. Primer sets were designed for PCR amplification of either the ~1100bp full-length (FL) *RARG* 3'UTR or two smaller regions (~300bp) within the *RARG* 3'UTR containing individual predicted miR-96 target sites (t1, t2). PCR amplicons were digested and ligated to RSV-pGL3-basic vector via T4 DNA Ligase in 1X T4 DNA Ligase Buffer (New England BioLabs, Inc.), using an insert to vector ratio of 2.6. Individual transformed *E.coli* colonies were expanded prior to plasmid isolation via E.Z.N.A® Plasmid Mini Kit (Omega), and inserts verified by sanger sequencing. RWPE1 cells were seeded in 96-well plates and then co-transfected with combinations of miR-96 or miR-control mimics (30nM), indicated RSV-pGL3 constructs (250ng), and pRL-CMV Renilla luciferase expressing vectors (25ng) via Lipofectamine® 2000 for 48 hr. Media was subsequently removed, cells washed with PBS, and both firefly and Renilla luciferase activity measured by Dual-Glo Luciferase Assay System (Promega). For each construct (FL, t1, t2,

empty), detected firefly luminescence was first normalized to Renilla luminescence, and then normalized luminescence was compared between miR-96 and miR-control transfected cells. Experiments were performed in technical triplicates, and experiment replicated a total of 5 times.

Stable knockdown of RARγ

Knockdown of RARγ in RWPE1, LNCaP and HPr1AR cells was achieved by stable selection after transduction with lentiviral shRNA constructs targeting *RARG*. Two targeting constructs (V2LHS_239272, V2LHS_239268) and one non-silencing control construct were selected from the V2LHS pGIPZ based lentiviral shRNA library (Thermo Fisher Scientific) for testing. Viral packaging and cellular infection was performed through the RPCI shRNA Resource. All pGIPZ containing cells were subsequently maintained in media supplemented with puromycin (2μg/mL), including during all experiments.

RWPE1-BAC-RARG-EGFP

BAC-RARG-EGFP construct (CTD-2644H7) was a generous gift of Dr. Kevin White (University of Chicago). RWPE1 cells were transfected with BAC-RARG-EGFP construct using Lipofectamine® 3000 and selected with G418 and consistently maintained under antibiotic selection for all subsequent passaging of cells and also during experiments.

Chromatin Immunoprecipitation

ChIP was performed in BAC-RARG-EGFP containing RWPE1 cells in the presence of CD437 (10nM, 2hr) or DMSO as previously described(8). The RARγ cistrome was analyzed with `Rsubread/csaw`(45), along with TF motif analyses (`MotifDb`). Binding site overlaps between RARγ and the other cistromes tested (`ChIPpeakAnno` and `bedtools`).

Biotin-miRNA pulldown

Approximately 20 million cells were transfected with either hsa-miR-96-5p or cel-miR-67 miRIDIAN miRNA mimics (30nM, 24hr) modified with a 3'biotin attached to the guide strand (Thermo Fisher Scientific) using Lipofectamine® 3000 Transfection Reagent (Invitrogen). Harvested cell pellets were resuspended in cell lysis buffer (10mM KCl, 1.5mM MgCl2, 10mM Tris-Cl pH 7.5, 5mM DTT, 0.5% Sigma-IGEPAL CA-630) containing SUPERase·In (Ambion) and 1x cOmplete Mini protease inhibitor (Roche) and cleared by centrifugation. 5% of cell lysate was collected to serve as lysate RNA input. Dynabeads® MyOne™ Streptavidin C1 (Thermo Fisher Scientific) were washed 3 times with bead wash buffer (5mM Tris-Cl pH 7.5, 0.5mM

EDTA, 1M NaCl), and then blocked (1μg/μL bovine serum albumin, 1μg/μL Yeast tRNA, 50U/mL RNaseOUT) for 2 hr. Resuspended beads were added 1:1 to cell lysate, and mixed for 30 minutes. Bead-lysate mixtures were collected with a magnetic rack, and bead-bi-miR complexes washed a total 3 times with wash buffer. Bead-bi-miR complexes and input control samples were resuspended in water and purified using the Qiagen RNeasy® Mini kit (Qiagen) according to manufacturer's RNA clean-up protocol. To concentrate samples for downstream analyses, eluted RNA was brought up to a total volume of 500μL in H_2O and filtered through Amicon® Ultra-0.5mL Centrifugal Filters (EMD Millipore) according to manufacturer's instructions. Subsequent amplification and labeling of 50ng of pulldown and input RNA was performed at the Roswell Park Cancer Institute Genomics Core Facility, using the Illumina® TotalPrep RNA Amplification kit, including a 14 hour incubation for the IVT step. Hybridization of cRNA samples onto the Illumina® Human HT-12v4 bead arrays, and successive scanning and raw intensity measurement extraction were also performed at the RPCI Genomics Core Facility.

miRNA prediction determination & TCGA miRNA analysis

To reveal putative NR-targeting miRNA, miRWalk, a comprehensive database on predicted and validate miRNA targets, was employed. If at least 5 out of 9 algorithms positively predicted an interaction, it was considered in subsequent analyses. MiRNA expression was queried in PCa tissue samples and matched normal tissue from TCGA cohort data as previously described(10). To examine if NR-targeting miRNA expression alterations significantly deviated from what would be expected by chance, bootstrapping approaches were utilized as previously described(10).

Microarray / RNA-seq analyses

Global changes in mRNA, biological triplicate samples per experimental condition were analyzed using Illumina microarray (Illumina HT12v4) or by RNA-seq (`limma`(46) or `DESeq2`(47)). For RNA-seq data, raw sequence reads were aligned to the human genome (hg19) using `tophat2`, and aligned reads translated to expression counts via `featurecounts`, followed by a standard `DESeq2` pipeline.

Functional annotation of shRARG defined gene sets

Functional annotations were performed using GSEA v3.0 and gene sets from the Molecular signatures database (MSigDB). Specifically, gene sets were compiled to assess enrichment of all BROAD Hallmark pathways, curated pathways (KEGG, BioCarta, Canonical, Reactome, Chemical/Genetic perturbations), and transcription factor motif gene sets. Additionally, several candidate gene sets were included from previous studies, including microarray analyses of

HPr1AR cells treated with DHT(48), compiled gene sets previously utilized to encompass androgen response in PCa patients(12), as well as gene sets differentiating basal from luminal prostate epithelial cells(49). In total, 4204 gene sets were queried.

To identify meta groups within enriched (NES > 1.8, FDR q-val < 0.05) gene sets, keywords from gene set identifiers were compiled, and frequency tables determined for all keywords across all gene sets and within enriched gene sets. To account for background frequencies of given terms across gene sets hypergeometric testing was used to determine if the frequency of key words within enriched gene sets was greater than expected.

Validation of miR-96 target sites & Functional annotation

Unbiased assessment of miRNA seed sequence binding motifs in experimentally determined miR-96 target transcript 3'UTR regions was performed using the MSigDB microRNA targets collection.Functional annotation of GO terms enriched in miR-96 target genes was accomplished via DAVID Bioinformatics Resources 6.7 (via BiNGO) and additionally by the topGO package implemented in R. Significantly enriched terms (FDR < 0.05) by both methods were simultaneously visualized using Cytoscape 3.2.0. Survival outcomes were determined using `Survival`.

AUTHORS CONTRIBUTIONS

Acknowledgements

LESC acknowledges support, in part, of Roswell Park Cancer Institute-University of Pittsburg Cancer Institute Ovarian Cancer Specialized Program of Research Excellence National Institutes of Health [P50CA159981-01A1].

MDL acknowledges support of Molecular Pharmacology and Experimental Therapeutics NRSA T32 program [T32CA009072] held at Roswell Park Cancer Institute.

MJC and *DJS* acknowledges support in part from the Prostate program of the Department of Defense Congressionally Directed Medical Research Programs [W81XWH-14-1-0608, W81XWH-11-2-0033] and the National Cancer Institute (NCI) grant P30CA016056 involving the use of Roswell Park Cancer Institute's Genomic Shared Resource.

MJC, GL, AR, HW and *PvdB* acknowledges support from the European Union-United States Atlantis Program [P116J090011].

MJC and *LESC* acknowledge support from the National Cancer Institute (NCI) grant P30CA016056 involving the use of OSUCCC The James, CCSG P30CA016058

RARγ State	Motif	Enrich.	E-Value
Apo	FOSB JUNB JUN	MEME	1.2e-80
	OTX2 PITX2 PITX1	MEME	9.2e-12
	RARB RARA RARG	MEME	2.4e-9
	ELF3 TFDP1 STAT1	MEME	3.2e-7
Holo	CPEB1 ONEC2 HXC10	MEME	1.5e-14
	FOSB JUNB JUN	MEME	3.3e-12
	HIC2 RREB1 PAX5	MEME	6.1e-7

Table 1: Summary of top motif enrichments in significant RARγ binding sites identified from ChIP-seq.

Figure Legends

Figure 1: Retinoid independent regulatory function of RARγ in prostate cells. (**A**) Relative proliferation of shRARG clones compared to vector controls in RWPE1 (left) and LNCaP (right) cells over time. Significant differences are indicated between control and RARγ knockdown cells ($p < 0.05$). (**B**) Cells were treated in triplicate with CD437 (RWPE1 - 10 nM; LNCaP- 250 nM, 24hr) or vehicle control and gene expression profiled via Illumina microarray (Illumina HT12v4). Volcano plots depicting expression changes upon RARγ knockdown (*apo* RARγ) or in response to RARγ specific ligand (CD437) (*holo* RARγ) in RWPE1 cells. Dotted lines indicate DEG thresholds (p.adj < 0.05, fold change of +/- 1.2), and red dots represent RARγ dependent DEGs. *Holo* RARγ were those genes that were significant in shCTL cells (shCTRL-CD437/shCTRL-DMSO) and not in shRARG cells cells. (**C**) Venn diagram depicting number of determined DEGs associated with *apo* RARγ and *holo* RARγ conditions. (**D**) Summary of significantly enriched pathways from GSEA (NES > 1.8, FDR q.val < 0.05) associated with *apo* RARγ and *holo* RARγ conditions in RWPE1 and LNCaP cells. Example enriched meta-groups amongst significant GSEA sets are indicated. Examples of top significant GSEA pathway enrichments observed (**E,F**) in RWPE1 cells and (**G**) in LNCaP cells. (**H**) Heatmap depicting the relative expression of a panel of androgen response genes defined previously by the TCGA consortium to reflect AR signaling(50).

Figure 2: The RARγ cistrome associates with androgen receptor and regulates genes associated with aggressive prostate cancer. Stable transfection of a bacterial artificial chromosome containing a fusion *RARG-EGFP* gene transcribed from the endogenous *RARG* promoter was undertaken to generate RWPE1-RARG-EGFP clones, followed by ChIP-Seq undertaken with an EGFP antibody. RWPE1-RARγ-EGFP cells were treated in triplicate with either CD437 (10 nM, 2 hr) or vehicle prior to ChIP-seq. (**A**) Cross profiling of significant *apo* RARγ ChIP-seq peaks (p.adj<0.1) and the indicated histone modifications from RWPE-1 (GSE63094) at genomic loci performed using the annotatePeaks.pl tool available from the HOMER (Hypergeometric Optimization of Motif EnRichment) suite. Upper panel is for the peaks at enhancer regions, and lower panel is TSS of RARγ annotated genes (**B**) Overlap of RARγ cistrome with publically available epigenetic datasets (H3K4me1 and H3K27ac (GSE63094) and DNAse sensitivity (GSM1541008). (**C**) Significance of *apo* RARγ peaks with publically available data; prostate enhancers (FANTOM; LNCaP AR, VCaP AR (GSE84432), ERα (GSE43985) and LNCaP NF-κB cistromes (GSE83860) (**D**) Illustration of binding site at the TSS of the KRT15 gene showing coincident binding with H3K4me1 and H3K27ac in RWPE-

1 cells, the ChromHMM track (grass green = low transcription; bright green = Active enhancer; red = Transcriptional enhancer ; blue = Active TSS ; pale yellow = Poised transcription; yellow = Poised enhancer). (**E**) The impact of RARγ knockdown on KRT15 from the microarray experiment in RWPE-1 cells (**Figure 1**). (**F**) Bootstrapping approach to test the statistical strength of relationships between genes annotated to be bound by RARγ (+/- 7.5 kb from the TSS) and modulated by shRARG (left) or in the presence of ligand (right). The red line is the mean observed fold change for the indicated gene set and the distribution is simulated data from the same background. (**G**) Heatmap of expression of annotated *apo* RARγ cistrome genes in the TCGA-PRAD cohort. Genes were filtered to identify those that were altered by more than 2 Z scores in 35% of tumors relative to normal samples. Cluster association grouped tumors that significantly distinguished higher Gleason Grade (Gleason_score >7), after adjusting for age. For each gene Kaplan-Meier curves were generated as time to biochemical progression and those genes which identify significantly (p.adj < 0.1) shorter disease free survival are indicated (Sig_survival). Pearson's Chi-squared test X-squared = 51.187, df = 35 (**G**). Illustrative Kaplan-Meier curve for *CYP11A1* expression depicting the significantly reduced time to 5 year biochemical recurrence (BCR) post radical prostatectomy.

Figure 3: RARγ governs androgen induced responses in non-malignant HPr1AR prostate epithelial cells. (**A**) Proliferation of HPr1AR-shCTL and HPr1AR-shRARG cells with or without the presence of 10 nM DHT for up to 96 hours. (**B**) HPr1AR-shCTL and HPr1AR-shRARG cells were treated in triplicate with DHT for 24h or vehicle control and gene expression profiled via RNA-seq. Volcano plot depicting DHT induced (10 nM, 24 hr) gene expression changes in HPr1AR-shCTL cells. Genes marked in red represent those that displayed differential regulation in RARγ knockdown cells. (**C**) Venn diagram representing the number of DEGs determined after DHT treatment in control and RARγ knockdown HPr1AR cells. (**D**) Heatmap depicting all enriched pathways related to DHT treatment (NES > 1.8, FDR q-val < 0.05). Select meta groups from keyword enrichment analysis are depicted as row annotations. The definitions of the groups are as follows; shCTL+DHT = shCTL+DHT/shCTL+EtOH, shRARG+DHT = shRARG+DHT/shRARG+EtOH, Apo-RARG (+DHT) = shRARG+DHT/shCTL+DHT. (**E**) Example of top significantly upregulated and (**F**) downregulated GSEA pathway enrichments upon DHT treatment. Enrichments are shown for each comparison, as well as an expression profile from a select gene from the respective gene set.

Figure 4: MicroRNA-96 directly targets and regulates *RARG* in prostate cells. (**A**) Cross-correlation matrices depicting the relationships between RARG expression and miR-96 cluster

members in PCa samples from either MSKCC or TCGA-PRAD cohorts. (**B**) Relative expression of miR-96 (bottom) and *RARG* (top) across 10 prostate cell lines representing different stages of PCa progression. The cell models examined comprised immortalized RWPE1 and HPr1AR non-malignant prostate epithelial cells, LNCaP, LAPC4 and EAA006 androgen sensitive PCa cells, MDAPCa2b, 22Rv1 and LNCaP-C42 CRPC cells, as well as PC3 and DU145 cells derived from distant metastases. (**C**) Correlation analyses of *RARG* with miR-96 over the course of palpable tumor (PT) development in TRAMP. (**D**) *RARG* expression (left panel) and RARγ protein expression (right panels) in RWPE1 cells after 48 hr transfections with miR-96 mimics or siRNA targeting *RARG*. (**E**) Luciferase assay assessing direct targeting of miR-96 to the full length (FL) RARG 3'UTR or individual predicted target sites (t1, t2) within the RARG 3'UTR. Either miR-96 or miR-CTL mimics (30 nM) were transfected into RWPE1 cells for 48 hours along with indicated RSV-pGL3 constructs and pRL-CMV Renilla luciferase expressing vectors, and luciferase activity measured by Dual-Glo Luciferase Assay System. (**F**) RWPE1 cells were pretreated with miR-CTL, miR-96 mimic (30 nM), or combination of miR-96 mimic and antagomiR-96 for 48 hours prior to 10 nM CD437 exposure for 24 hours, and candidate transcripts measured by RT-qPCR. Induction relative to untreated control for each condition is shown, and significance relative to shCTL is noted. (**G**) Cell proliferation was measured in RWPE-1 (left) and LNCaP (right) cells for up to 120 hours post-transfection with either miR-96 or non-targeting control (NC) mimics.

Figure 5: The miR-96 targetome centers on a RARγ-network associated with aggressive prostate cancer (**A**) LNCaP cells were transfected with bi-miR-96 or bi-cel-miR-67 (non-targeting control, bi-miR-NC) (30 nM) 24 hr prior to cell lysis. From triplicates, input (5% of cell lysate) and streptavidin pulldown RNA were isolated and analyzed by Illumina microarray (Illumina HT12v4). Volcano plot depicting the enrichment of all genes in bi-miR-96 pulldown over input in LNCaP cells. Genes marked in red (n = 389) were considered experimentally determined miR-96 direct targets, as they were significantly enriched (FC > 1.2, p.adj < 0.05) in bi-miR-96 pulldown but not in bi-miR-NC pulldown. (**B**) Venn diagram representing the overlap of miR-96 targetomes in LNCaP and RWPE1 cells. (**C**) Example of top significantly enriched GSEA pathway from unbiased enrichment analysis of bi-miR-96 samples in LNCaP cells (pulldown/input) (top), and summary of top miRNA seed sequence matches in 3'UTR regions of experimentally determined miR-96 targets using the GSEA-MSigDB microRNA targets tool (bottom). (**D**) Either bi-miR-96 or non-biotinylated miR-96 mimics, and respective control mimics, were transfected (30nM) in LNCaP cells for 48 hr and target gene expression examined. *CDH1* was assessed as a negative control, and specific targets were chosen either

as they were either previously validated (*FOXO1*, *RARG*) and were significantly enriched in bi-miR assay. Significance is noted ($p < 0.05$), for comparisons of target transcripts in biotinylated and non-biotinylated miR-96 relative to respective controls. (**E**) Cumulative distribution plot comparing the correlations (Pearson's r) between miR-96 and all detectable genes from bi-miR-pulldown assay (n = 10,827, black) in TCGA-PRAD cohort samples to the correlations of validated targets (n = 389, red) across the same samples. Significant difference between distributions is determined by Kolmogorov-Smirnov test. (**F**). Heatmap depicting expression of annotated LNCaP miR-96 targetome genes in the TCGA-PRAD cohort. Genes were filtered to identify those genes that were altered by more than 2 Zscores in 35% of tumors relative to normal samples. Cluster association grouped tumors into groups that significantly distinguished invasive tumors (Path_N N0 or N1), after adjusting for age. For each gene Kaplan-Meier curves were generated as time to biochemical progression and those genes which identify significantly shorter disease free survival are indicated (Sig_Survival) (p.adj <0.01). Also indicated is the functional relationship of the gene to RARγ as membership of the RARγ network (RARg_Network).

Figure 6: A miR-96/RARγ network associates with aggressive prostate cancer. (**A**) TCGA-PRAD cohort tumor samples were separated based on expression of RARγ, TACC1 and miR-96 (based on lower/upper tertile expression) to generate RARγ/TACC1$_{low}$, miR-96$_{high}$ (n = 60) and RARγ/TACC1$_{high}$, miR-96$_{low}$ (n = 66) tumors and differential expression undertaken. (**B**) Filtering the differentially expressed 1728 gene sets as in **Figure 2G** revealed which were most altered in the TCGA-PRAD cohort. These are represented as a heatmap in which tumor clusters significantly associated, after adjusting for age with higher Gleason Grade (Gleason_score >7). These clusters also significantly identified patients who experienced treatment failure and worse disease free survival following radical prostatectomy (X_RFS_IND; log-rank test p-val = 0.026). Individual genes were annotated by their relationship to RARγ binding (RARg_ChIP), RARγ-dependent DHT regulation (RARg_AR), and enrichment in the Liu prostate cancer gene set (Liu_Down). (**C**) SOX15 is bound by RARγ and also a RARγ-dependent AR regulated target. Illustration of RARγ binding site at SOX15 gene showing coincident binding with H3K4me1 and H3K27ac in RWPE-1 cells, the ChromHMM track (cyan= TSS flanking; grass green = low transcription; bright green = Active enhancer; red = Transcriptional enhancer ; blue = Active TSS ; pale yellow = Poised transcription)

References

1. Kerr JF, Wyllie AH, Currie AR. Apoptosis: a basic biological phenomenon with wide-ranging implications in tissue kinetics. Br J Cancer **1972**;26(4):239-57.
2. Malinen M, Niskanen EA, Kaikkonen MU, Palvimo JJ. Crosstalk between androgen and pro-inflammatory signaling remodels androgen receptor and NF-kappaB cistrome to reprogram the prostate cancer cell transcriptome. Nucleic Acids Res **2017**;45(2):619-30 doi 10.1093/nar/gkw855.
3. Zhang J, Gonit M, Salazar MD, Shatnawi A, Shemshedini L, Trumbly R*, et al.* C/EBPalpha redirects androgen receptor signaling through a unique bimodal interaction. Oncogene **2010**;29(5):723-38 doi 10.1038/onc.2009.373.
4. Llukani E, Katz BF, Agalliu I, Lightfoot A, Yu SS, Kathrins M*, et al.* Low levels of serum testosterone in middle-aged men impact pathological features of prostate cancer. Prostate Int **2017**;5(1):17-23 doi 10.1016/j.prnil.2016.12.003.
5. Chatagnon A, Veber P, Morin V, Bedo J, Triqueneaux G, Semon M*, et al.* RAR/RXR binding dynamics distinguish pluripotency from differentiation associated cis-regulatory elements. Nucleic Acids Res **2015**;43(10):4833-54 doi 10.1093/nar/gkv370.
6. Boergesen M, Pedersen TA, Gross B, van Heeringen SJ, Hagenbeek D, Bindesboll C*, et al.* Genome-wide profiling of liver X receptor, retinoid X receptor, and peroxisome proliferator-activated receptor alpha in mouse liver reveals extensive sharing of binding sites. Mol Cell Biol **2012**;32(4):852-67 doi 10.1128/MCB.06175-11.
7. Sun J, Wang Y, Li Y, Zhao G. Downregulation of PPARgamma by miR-548d-5p suppresses the adipogenic differentiation of human bone marrow mesenchymal stem cells and enhances their osteogenic potential. J Transl Med **2014**;12:168 doi 10.1186/1479-5876-12-168.
8. Thorne JL, Maguire O, Doig CL, Battaglia S, Fehr L, Sucheston LE*, et al.* Epigenetic control of a VDR-governed feed-forward loop that regulates p21(waf1/cip1) expression and function in non-malignant prostate cells. Nucleic Acids Res **2011**;39(6):2045-56 doi 10.1093/nar/gkq875.
9. Long MD, Thorne JL, Russell J, Battaglia S, Singh PK, Sucheston-Campbell LE*, et al.* Cooperative behavior of the nuclear receptor superfamily and its deregulation in prostate cancer. Carcinogenesis **2014**;35(2):262-71 doi 10.1093/carcin/bgt334.
10. Long MD, Campbell MJ. Pan-cancer analyses of the nuclear receptor superfamily. Nucl Receptor Res **2015**;2 doi 10.11131/2015/101182.
11. Taylor BS, Schultz N, Hieronymus H, Gopalan A, Xiao Y, Carver BS*, et al.* Integrative genomic profiling of human prostate cancer. Cancer Cell **2010**;18(1):11-22 doi 10.1016/j.ccr.2010.05.026.
12. Cancer Genome Atlas Research N. The Molecular Taxonomy of Primary Prostate Cancer. Cell **2015**;163(4):1011-25 doi 10.1016/j.cell.2015.10.025.
13. Hua S, Kittler R, White KP. Genomic antagonism between retinoic acid and estrogen signaling in breast cancer. Cell **2009**;137(7):1259-71 doi 10.1016/j.cell.2009.04.043.
14. Sallari RC, Sinnot-Armstrong, N.A., French, J.D., Kron, K.J., Ho, J., Moore, J. H., Stambolic, V., Edwards, S. L., Lupien, M., Kellis, M.,. Convergence of dispersed regulatory mutations predicts driver genes in prostate cancer. BioRxiv **2017** doi doi: https://doi.org/10.1101/097451.
15. Andersson R, Gebhard C, Miguel-Escalada I, Hoof I, Bornholdt J, Boyd M*, et al.* An atlas of active enhancers across human cell types and tissues. Nature **2014**;507(7493):455-61 doi 10.1038/nature12787.
16. Tan PY, Chang CW, Chng KR, Wansa KD, Sung WK, Cheung E. Integration of regulatory networks by NKX3-1 promotes androgen-dependent prostate cancer survival. Mol Cell Biol **2012**;32(2):399-414 doi 10.1128/MCB.05958-11.

17. Dhiman VK, Attwood K, Campbell MJ, Smiraglia DJ. Hormone stimulation of androgen receptor mediates dynamic changes in DNA methylation patterns at regulatory elements. Oncotarget **2015**;6(40):42575-89 doi 10.18632/oncotarget.6471.
18. Dweep H, Sticht C, Pandey P, Gretz N. miRWalk--database: prediction of possible miRNA binding sites by "walking" the genes of three genomes. Journal of biomedical informatics **2011**;44(5):839-47 doi 10.1016/j.jbi.2011.05.002.
19. Kwabi-Addo B, Giri D, Schmidt K, Podsypanina K, Parsons R, Greenberg N*, et al.* Haploinsufficiency of the Pten tumor suppressor gene promotes prostate cancer progression. Proc Natl Acad Sci U S A **2001**;98(20):11563-8 doi 10.1073/pnas.201167798.
20. Haflidadottir BS, Larne O, Martin M, Persson M, Edsjo A, Bjartell A*, et al.* Upregulation of miR-96 enhances cellular proliferation of prostate cancer cells through FOXO1. PLoS One **2013**;8(8):e72400 doi 10.1371/journal.pone.0072400.
21. Tan SM, Lieberman J. Capture and Identification of miRNA Targets by Biotin Pulldown and RNA-seq. Methods Mol Biol **2016**;1358:211-28 doi 10.1007/978-1-4939-3067-8_13.
22. Jones HE, Eaton CL, Barrow D, Dutkowski C, Griffiths K. Response of cell growth and retinoic acid receptor expression to retinoic acid in neoplastic and non-neoplastic prostate cell lines. Prostate **1997**;30(3):174-82.
23. Guyot R, Vincent S, Bertin J, Samarut J, Ravel-Chapuis P. The transforming acidic coiled coil (TACC1) protein modulates the transcriptional activity of the nuclear receptors TR and RAR. BMC Mol Biol **2010**;11:3 doi 10.1186/1471-2199-11-3.
24. Luo Z, Gao X, Lin C, Smith ER, Marshall SA, Swanson SK*, et al.* Zic2 is an enhancer-binding factor required for embryonic stem cell specification. Mol Cell **2015**;57(4):685-94 doi 10.1016/j.molcel.2015.01.007.
25. Qiu JJ, Lu X, Zeisig BB, Ma Z, Cai X, Chen S*, et al.* Leukemic transformation by the APL fusion protein PRKAR1A-RAR{alpha} critically depends on recruitment of RXR{alpha}. Blood **2010**;115(3):643-52 doi 10.1182/blood-2009-07-232652.
26. Ozpolat B, Akar U, Zorrilla-Calancha I, Vivas-Mejia P, Acevedo-Alvarez M, Lopez-Berestein G. Death-associated protein 5 (DAP5/p97/NAT1) contributes to retinoic acid-induced granulocytic differentiation and arsenic trioxide-induced apoptosis in acute promyelocytic leukemia. Apoptosis **2008**;13(7):915-28 doi 10.1007/s10495-008-0222-9.
27. Johannesson M, Stahlberg A, Ameri J, Sand FW, Norrman K, Semb H. FGF4 and retinoic acid direct differentiation of hESCs into PDX1-expressing foregut endoderm in a time- and concentration-dependent manner. PLoS One **2009**;4(3):e4794 doi 10.1371/journal.pone.0004794.
28. Liu P, Ramachandran S, Ali Seyed M, Scharer CD, Laycock N, Dalton WB*, et al.* Sex-determining region Y box 4 is a transforming oncogene in human prostate cancer cells. Cancer Res **2006**;66(8):4011-9 doi 10.1158/0008-5472.CAN-05-3055.
29. Kinzler KW, Nilbert MC, Vogelstein B, Bryan TM, Levy DB, Smith KJ*, et al.* Identification of a gene located at chromosome 5q21 that is mutated in colorectal cancers. Science **1991**;251(4999):1366-70.
30. Chang SN, Lee JM, Oh H, Park JH. Glutathione Peroxidase 3 Inhibits Prostate Tumorigenesis in TRAMP Mice. Prostate **2016**;76(15):1387-98 doi 10.1002/pros.23223.
31. Thu KL, Radulovich N, Becker-Santos DD, Pikor LA, Pusic A, Lockwood WW*, et al.* SOX15 is a candidate tumor suppressor in pancreatic cancer with a potential role in Wnt/beta-catenin signaling. Oncogene **2014**;33(3):279-88 doi 10.1038/onc.2012.595.
32. Lohnes D, Kastner P, Dierich A, Mark M, LeMeur M, Chambon P. Function of retinoic acid receptor gamma in the mouse. Cell **1993**;73(4):643-58.

33. Roadmap Epigenomics C, Kundaje A, Meuleman W, Ernst J, Bilenky M, Yen A*, et al.* Integrative analysis of 111 reference human epigenomes. Nature **2015**;518(7539):317-30 doi 10.1038/nature14248.
34. Simandi Z, Horvath A, Wright LC, Cuaranta-Monroy I, De Luca I, Karolyi K*, et al.* OCT4 Acts as an Integrator of Pluripotency and Signal-Induced Differentiation. Mol Cell **2016**;63(4):647-61 doi 10.1016/j.molcel.2016.06.039.
35. Chen CF, Goyette P, Lohnes D. RARgamma acts as a tumor suppressor in mouse keratinocytes. Oncogene **2004**;23(31):5350-9 doi 10.1038/sj.onc.1207682.
36. Kashyap V, Laursen KB, Brenet F, Viale AJ, Scandura JM, Gudas LJ. RARgamma is essential for retinoic acid induced chromatin remodeling and transcriptional activation in embryonic stem cells. J Cell Sci **2013**;126(Pt 4):999-1008 doi 10.1242/jcs.119701.
37. Campbell MJ, Park S, Uskokovic MR, Dawson MI, Koeffler HP. Expression of retinoic acid receptor-beta sensitizes prostate cancer cells to growth inhibition mediated by combinations of retinoids and a 19-nor hexafluoride vitamin D3 analog. Endocrinology **1998**;139(4):1972-80 doi 10.1210/endo.139.4.5943.
38. Itkonen HM, Brown M, Urbanucci A, Tredwell G, Ho Lau C, Barfeld S*, et al.* Lipid degradation promotes prostate cancer cell survival. Oncotarget **2017**;8(24):38264-75 doi 10.18632/oncotarget.16123.
39. Zhang S, Yu M, Liu C, Wang L, Hu Y, Bai Y*, et al.* MIR-34c regulates mouse embryonic stem cells differentiation into male germ-like cells through RARg. Cell biochemistry and function **2012**;30(8):623-32 doi 10.1002/cbf.2922.
40. Tsai YC, Chen WY, Siu MK, Tsai HY, Yin JJ, Huang J*, et al.* Epidermal growth factor receptor signaling promotes metastatic prostate cancer through microRNA-96-mediated downregulation of the tumor suppressor ETV6. Cancer Lett **2017**;384:1-8 doi 10.1016/j.canlet.2016.10.014.
41. Mo W, Zhang J, Li X, Meng D, Gao Y, Yang S*, et al.* Identification of novel AR-targeted microRNAs mediating androgen signalling through critical pathways to regulate cell viability in prostate cancer. PLoS One **2013**;8(2):e56592 doi 10.1371/journal.pone.0056592.
42. Torrano V, Valcarcel-Jimenez L, Cortazar AR, Liu X, Urosevic J, Castillo-Martin M*, et al.* The metabolic co-regulator PGC1alpha suppresses prostate cancer metastasis. Nat Cell Biol **2016**;18(6):645-56 doi 10.1038/ncb3357.
43. Spahn M, Kneitz S, Scholz CJ, Stenger N, Rudiger T, Strobel P*, et al.* Expression of microRNA-221 is progressively reduced in aggressive prostate cancer and metastasis and predicts clinical recurrence. Int J Cancer **2010**;127(2):394-403 doi 10.1002/ijc.24715.
44. Gentleman RC, Carey VJ, Bates DM, Bolstad B, Dettling M, Dudoit S*, et al.* Bioconductor: open software development for computational biology and bioinformatics. Genome Biol **2004**;5(10):R80 doi 10.1186/gb-2004-5-10-r80.
45. Lun AT, Smyth GK. csaw: a Bioconductor package for differential binding analysis of ChIP-seq data using sliding windows. Nucleic Acids Res **2016**;44(5):e45 doi 10.1093/nar/gkv1191.
46. Ritchie ME, Phipson B, Wu D, Hu Y, Law CW, Shi W*, et al.* limma powers differential expression analyses for RNA-sequencing and microarray studies. Nucleic Acids Res **2015**;43(7):e47 doi 10.1093/nar/gkv007.
47. Love MI, Huber W, Anders S. Moderated estimation of fold change and dispersion for RNA-seq data with DESeq2. Genome Biol **2014**;15(12):550 doi 10.1186/s13059-014-0550-8.
48. Bolton EC, So AY, Chaivorapol C, Haqq CM, Li H, Yamamoto KR. Cell- and gene-specific regulation of primary target genes by the androgen receptor. Genes Dev **2007**;21(16):2005-17 doi 10.1101/gad.1564207.

49. Zhang D, Park D, Zhong Y, Lu Y, Rycaj K, Gong S*, et al.* Stem cell and neurogenic gene-expression profiles link prostate basal cells to aggressive prostate cancer. Nat Commun **2016**;7:10798 doi 10.1038/ncomms10798.
50. Cancer Genome Atlas Research Network. Electronic address scmo, Cancer Genome Atlas Research N. The Molecular Taxonomy of Primary Prostate Cancer. Cell **2015**;163(4):1011-25 doi 10.1016/j.cell.2015.10.025.

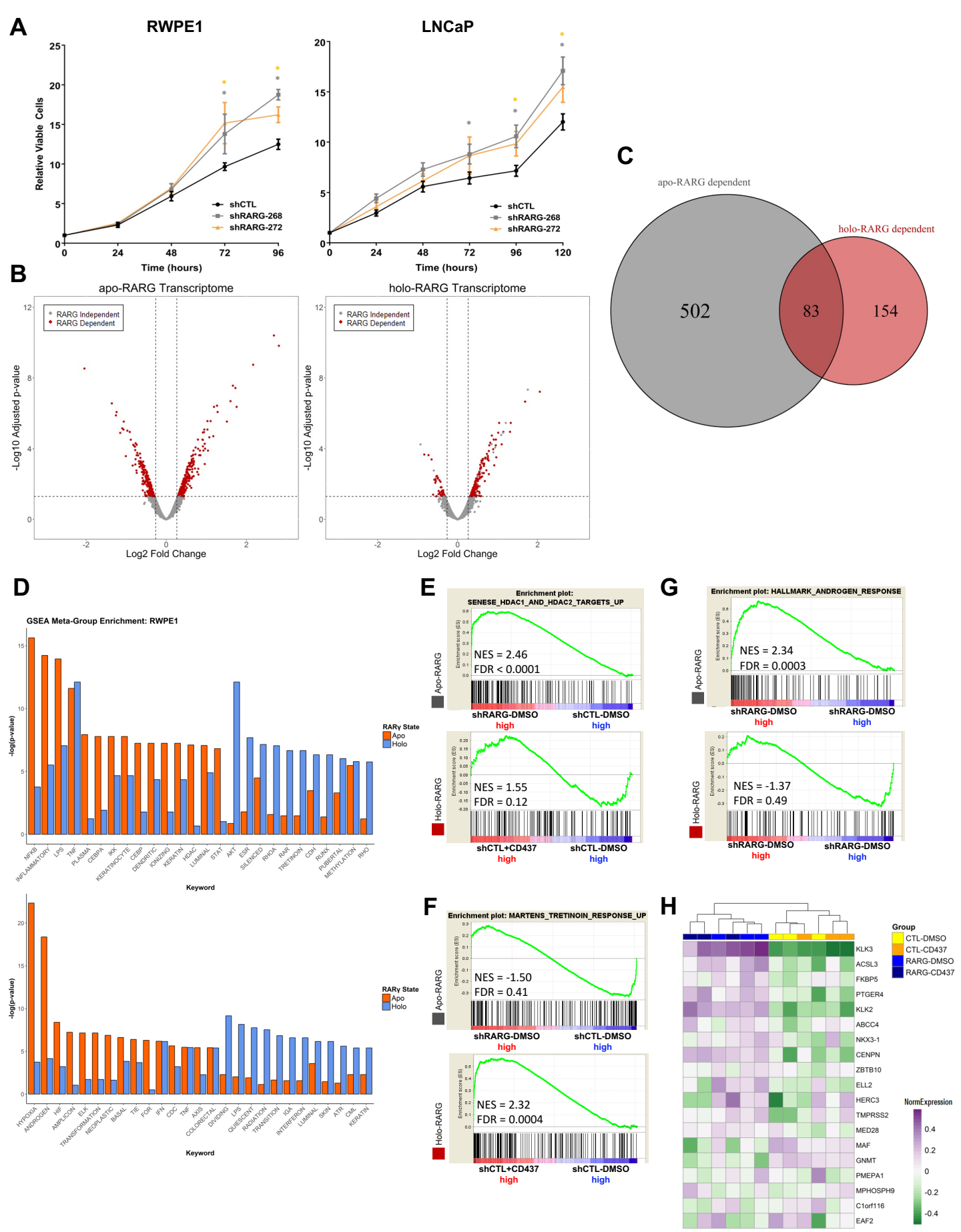
A
RWPE1
LNCaP
Relative Viable Cells
Time (hours)
shCTL
shRARG-268
shRARG-272
B
apo-RARG Transcriptome
holo-RARG Transcriptome
RARG Independent
RARG Dependent
-Log10 Adjusted p-value
Log2 Fold Change
C
apo-RARG dependent
holo-RARG dependent
502
83
154
D
GSEA Meta-Group Enrichment: RWPE1
-log(p-value)
RARγ State
Apo
Holo
Keyword
NFKB
INFLAMMATORY
LPS
TNF
PLASMA
CEBPA
IKK
KERATINOCYTE
CEBP
DENDRITIC
IONIZING
KERATIN
HDAC
LUMINAL
STAT
AKT
ESR
SILENCED
RHOA
RAR
TRETINOIN
CDH
RUNX
PUBERTAL
METHYLATION
RHO
HYPOXIA
ANDROGEN
HIF
AMPLICON
ELK
TRANSFORMATION
NEOPLASTIC
BASAL
TIE
FOR
IFN
CDC
TNF
AXIS
COLORECTAL
DIVIDING
LPS
QUIESCENT
RADIATION
TRANSITION
IGA
INTERFERON
LUMINAL
SKIN
ATR
CML
KERATIN
E
Enrichment plot: SENESE_HDAC1_AND_HDAC2_TARGETS_UP
Apo-RARG
NES = 2.46
FDR < 0.0001
shRARG-DMSO high
shCTL-DMSO high
Holo-RARG
NES = 1.55
FDR = 0.12
shCTL+CD437 high
shCTL-DMSO high
G
Enrichment plot: HALLMARK_ANDROGEN_RESPONSE
Apo-RARG
NES = 2.34
FDR = 0.0003
shRARG-DMSO high
shRARG-DMSO high
Holo-RARG
NES = -1.37
FDR = 0.49
shRARG-DMSO high
shRARG-DMSO high
F
Enrichment plot: MARTENS_TRETINOIN_RESPONSE_UP
Apo-RARG
NES = -1.50
FDR = 0.41
shRARG-DMSO high
shCTL-DMSO high
Holo-RARG
NES = 2.32
FDR = 0.0004
shCTL+CD437 high
shCTL-DMSO high
H
Group
CTL-DMSO
CTL-CD437
RARG-DMSO
RARG-CD437
KLK3
ACSL3
FKBP5
PTGER4
KLK2
ABCC4
NKX3-1
CENPN
ZBTB10
ELL2
HERC3
TMPRSS2
MED28
MAF
GNMT
PMEPA1
MPHOSPH9
C1orf116
EAF2
NormExpression
0.4
0.2
0
-0.2
-0.4

Figure 1

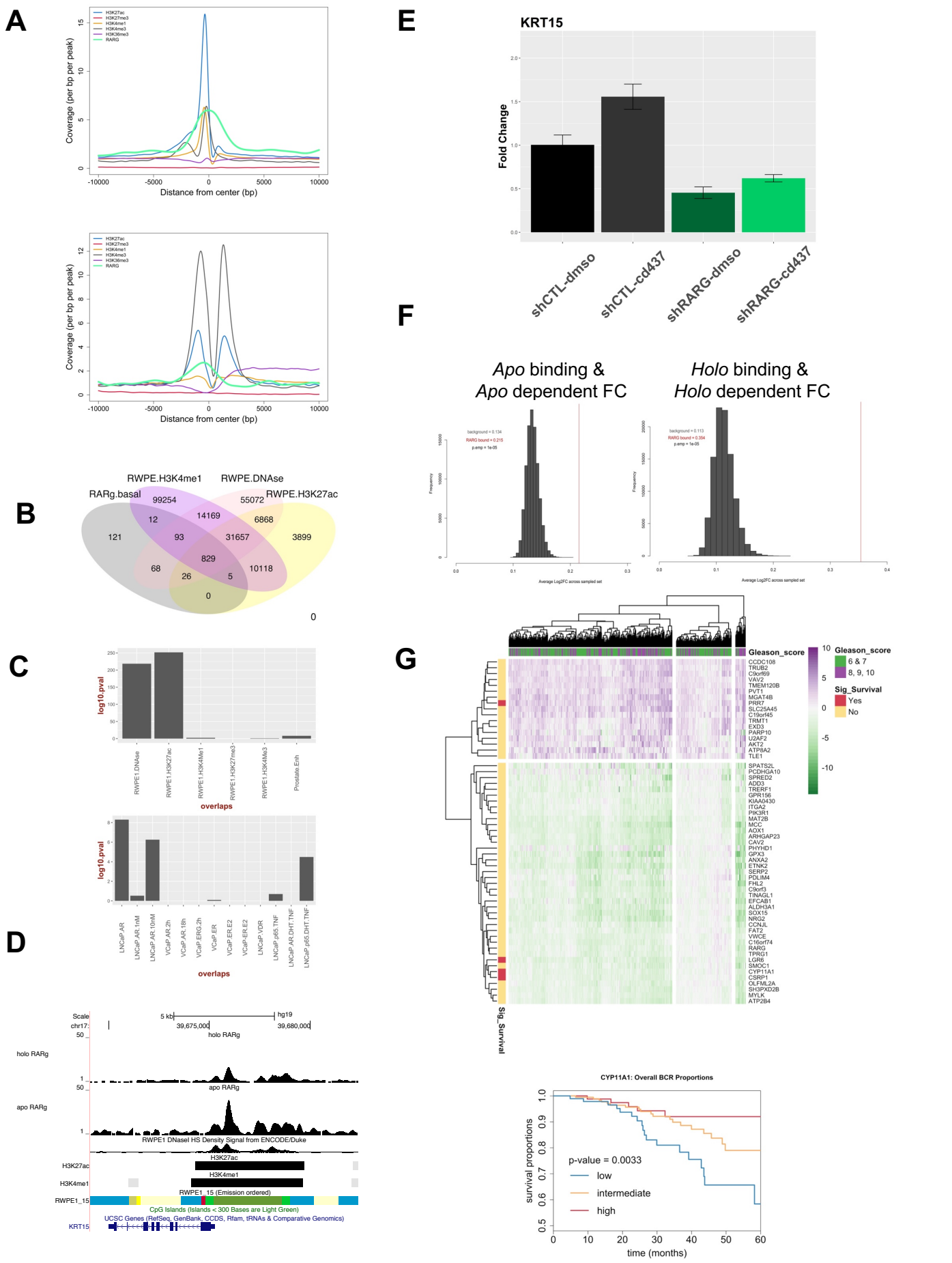
A
H3K27ac
H3K27me3
H3K4me1
H3K4me3
H3K36me3
RARG
Coverage (per bp per peak)
Distance from center (bp)
B
RWPE.H3K4me1
RWPE.DNAse
RARg.basal
RWPE.H3K27ac
99254
55072
12
14169
6868
121
93
31657
3899
829
68
26
5
10118
0
C
log10.pval
RWPE1.DNAse
RWPE1.H3K27ac
RWPE1.H3K4Me1
RWPE1.H3K27me3
RWPE1.H3K4Me3
Prostate.Enh
overlaps
LNCaP.AR
LNCaP.AR.1nM
LNCaP.AR.10nM
VCaP.AR.2h
VCaP.AR.18h
VCaP.ERG.2h
VCaP.ER
VCaP.ER.E2
VCaP.ER.E2
LNCaP.VDR
LNCaP.p65.TNF
LNCaP.AR.DHT.TNF-
LNCaP.p65.DHT.TNF-
D
Scale
chr17:
5 kb
hg19
39,675,000
39,680,000
holo RARg
apo RARg
RWPE1 DNaseI HS Density Signal from ENCODE/Duke
H3K27ac
H3K4me1
RWPE1_15 (Emission ordered)
CpG Islands (Islands < 300 Bases are Light Green)
UCSC Genes (RefSeq, GenBank, CCDS, Rfam, tRNAs & Comparative Genomics)
KRT15
E
KRT15
Fold Change
shCTL-dmso
shCTL-cd437
shRARG-dmso
shRARG-cd437
F
Apo binding &
Apo dependent FC
Holo binding &
Holo dependent FC
background = 0.134
RARG bound = 0.215
p.emp = 1e-05
background = 0.113
RARG bound = 0.354
p.emp = 1e-05
Frequency
Average Log2FC across sampled set
G
Gleason_score
6 & 7
8, 9, 10
Sig_Survival
Yes
No
CCDC108
TRUB2
C9orf69
VAV2
TMEM120B
PVT1
MGAT4B
PRR7
SLC25A45
C19orf45
TRMT1
EXD3
PARP10
U2AF2
AKT2
ATP8A2
TLE1
SPATS2L
PCDHGA10
SPRED2
ADD3
TRERF1
GPR156
KIAA0430
ITGA2
PIK3R1
MAT2B
MCC
AOX1
ARHGAP23
CAV2
PHYHD1
GPX3
ANXA2
ETNK2
SERP2
PDLIM4
FHL2
C9orf3
TINAGL1
EFCAB1
ALDH3A1
SOX15
NRG2
CCNJL
FAT2
VWCE
C16orf74
RARG
TPRG1
LGR6
SMOC1
CYP11A1
CSRP1
OLFML2A
SH3PXD2B
MYLK
ATP2B4
CYP11A1: Overall BCR Proportions
p-value = 0.0033
low
intermediate
high
survival proportions
time (months)

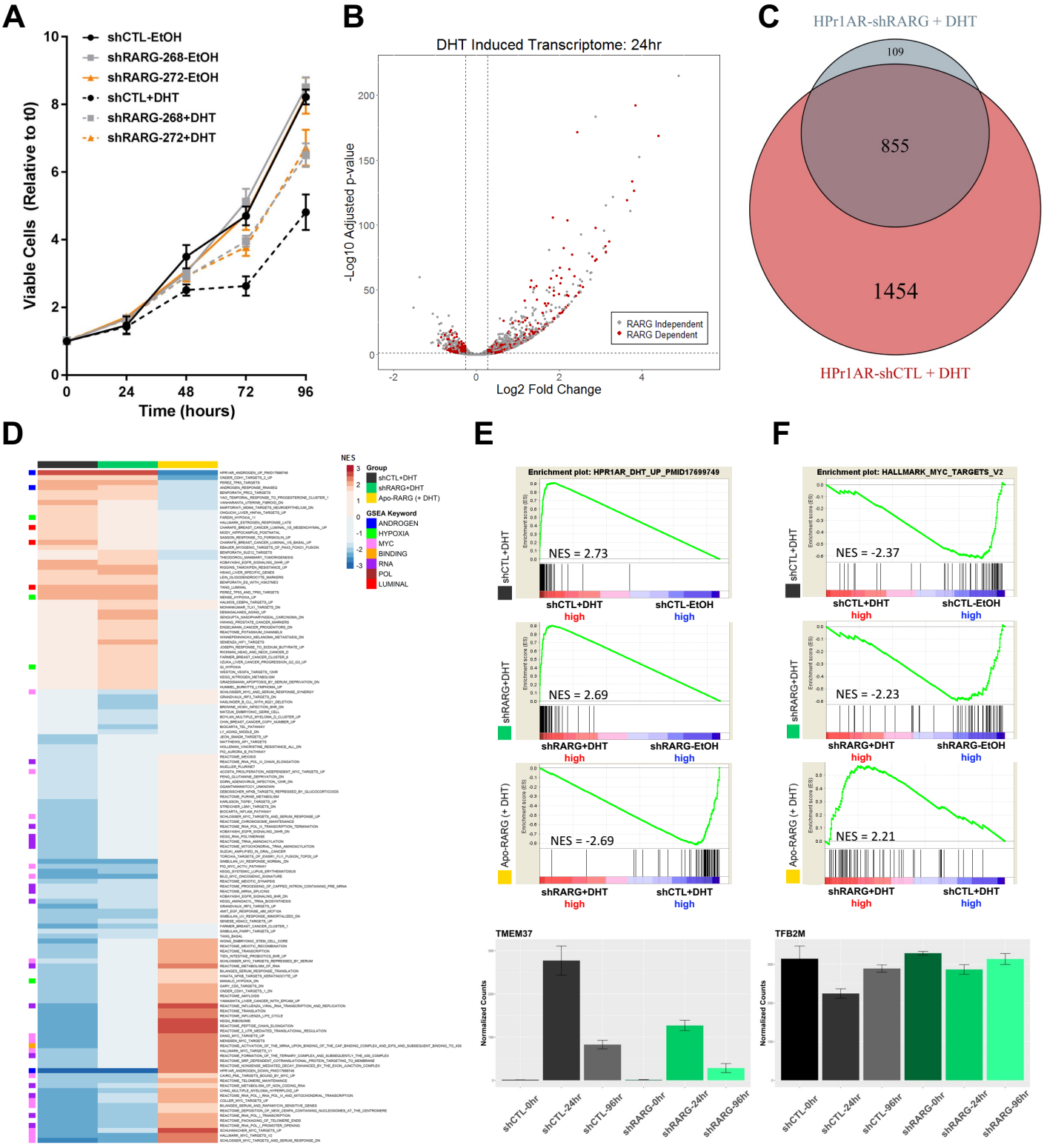
A
shCTL-EtOH
shRARG-268-EtOH
shRARG-272-EtOH
shCTL+DHT
shRARG-268+DHT
shRARG-272+DHT
Viable Cells (Relative to t0)
Time (hours)
B
DHT Induced Transcriptome: 24hr
-Log10 Adjusted p-value
Log2 Fold Change
RARG Independent
RARG Dependent
C
HPr1AR-shRARG + DHT
109
855
1454
HPr1AR-shCTL + DHT
D
NES
Group
shCTL+DHT
shRARG+DHT
Apo-RARG (+ DHT)
GSEA Keyword
ANDROGEN
HYPOXIA
MYC
BINDING
RNA
POL
LUMINAL
E
Enrichment plot: HPR1AR_DHT_UP_PMID17699749
NES = 2.73
NES = 2.69
NES = -2.69
shCTL+DHT high
shCTL-EtOH high
shRARG+DHT high
shRARG-EtOH high
F
Enrichment plot: HALLMARK_MYC_TARGETS_V2
NES = -2.37
NES = -2.23
NES = 2.21
TMEM37
TFB2M
Normalized Counts
shCTL-0hr
shCTL-24hr
shCTL-96hr
shRARG-0hr
shRARG-24hr
shRARG-96hr

Figure 3

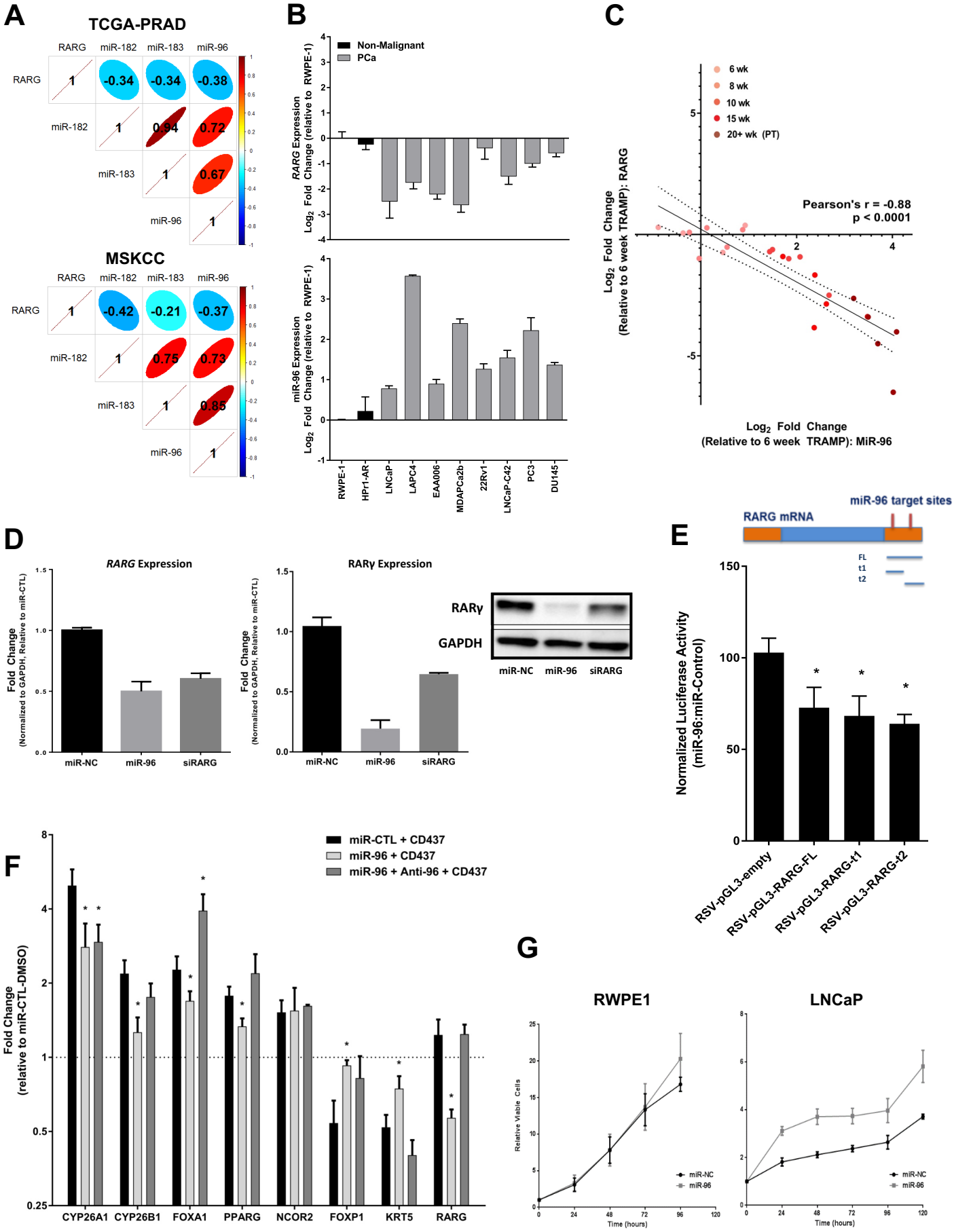
A
TCGA-PRAD
RARG
miR-182
miR-183
miR-96
1
-0.34
-0.34
-0.38
0.94
0.72
0.67
MSKCC
-0.42
-0.21
-0.37
0.75
0.73
0.85
B
Non-Malignant
PCa
RARG Expression
Log2 Fold Change (relative to RWPE-1)
miR-96 Expression
RWPE-1
HPr1-AR
LNCaP
LAPC4
EAA006
MDAPCa2b
22Rv1
LNCaP-C42
PC3
DU145
C
6 wk
8 wk
10 wk
15 wk
20+ wk (PT)
Pearson's r = -0.88
p < 0.0001
Log2 Fold Change
(Relative to 6 week TRAMP): RARG
Log2 Fold Change
(Relative to 6 week TRAMP): MiR-96
D
RARG Expression
Fold Change
(Normalized to GAPDH, Relative to miR-CTL)
miR-NC
miR-96
siRARG
RARγ Expression
RARγ
GAPDH
E
miR-96 target sites
RARG mRNA
FL
t1
t2
Normalized Luciferase Activity
(miR-96:miR-Control)
RSV-pGL3-empty
RSV-pGL3-RARG-FL
RSV-pGL3-RARG-t1
RSV-pGL3-RARG-t2
F
miR-CTL + CD437
miR-96 + CD437
miR-96 + Anti-96 + CD437
Fold Change
(relative to miR-CTL-DMSO)
CYP26A1
CYP26B1
FOXA1
PPARG
NCOR2
FOXP1
KRT5
RARG
G
RWPE1
LNCaP
Relative Viable Cells
Time (hours)
miR-NC
miR-96

Figure 4

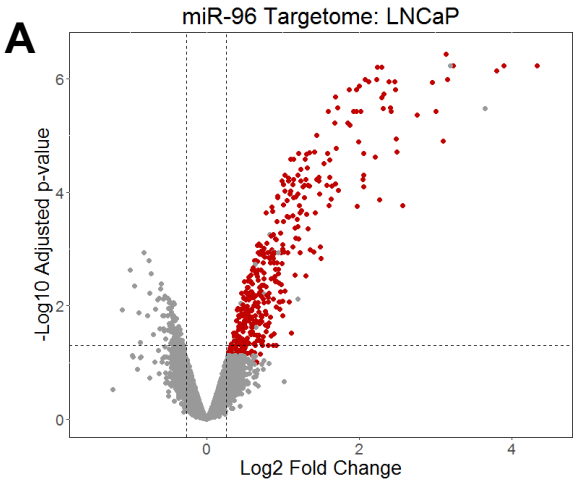
A
miR-96 Targetome: LNCaP
-Log10 Adjusted p-value
Log2 Fold Change

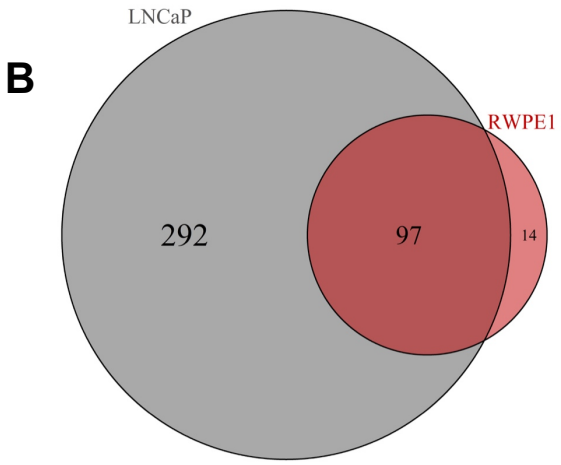
B
LNCaP
RWPE1
292
97
14

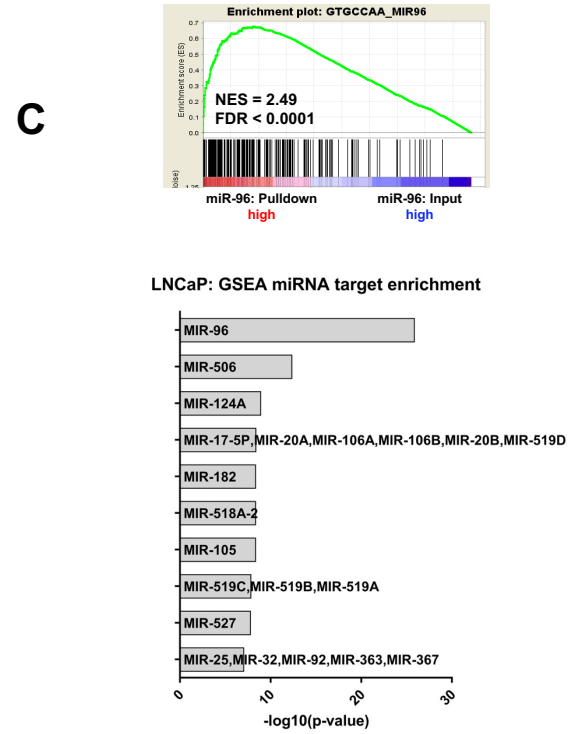
C
Enrichment plot: GTGCCAA_MIR96
NES = 2.49
FDR < 0.0001
miR-96: Pulldown
high
miR-96: Input
high
LNCaP: GSEA miRNA target enrichment
MIR-96
MIR-506
MIR-124A
MIR-17-5P,MIR-20A,MIR-106A,MIR-106B,MIR-20B,MIR-519D
MIR-182
MIR-518A-2
MIR-105
MIR-519C,MIR-519B,MIR-519A
MIR-527
MIR-25,MIR-32,MIR-92,MIR-363,MIR-367
-log10(p-value)

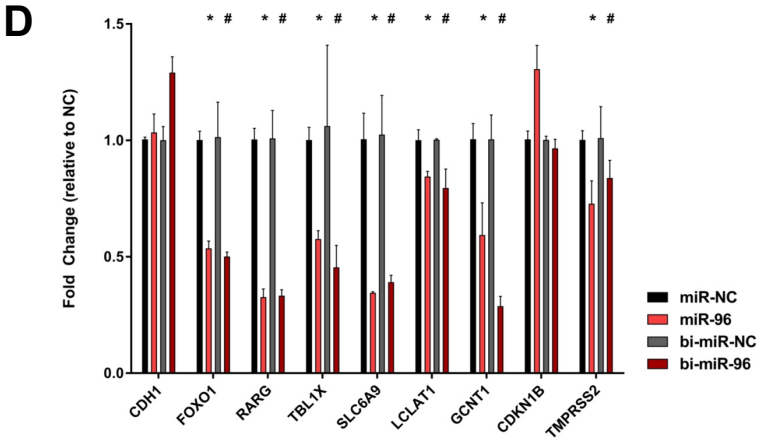
D
Fold Change (relative to NC)
CDH1
FOXO1
RARG
TBL1X
SLC6A9
LCLAT1
GCNT1
CDKN1B
TMPRSS2
miR-NC
miR-96
bi-miR-NC
bi-miR-96

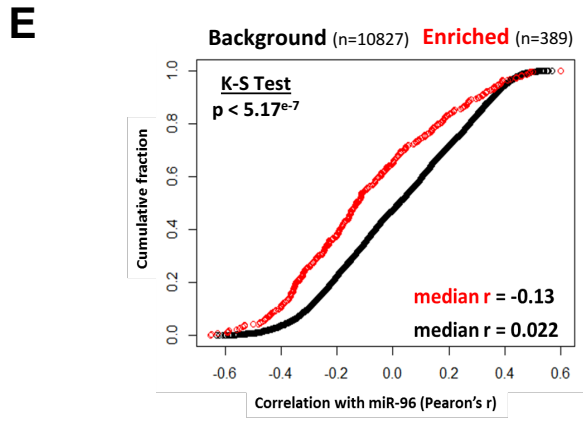
E
Background (n=10827) Enriched (n=389)
K-S Test
p < 5.17e-7
median r = -0.13
median r = 0.022
Cumulative fraction
Correlation with miR-96 (Pearon's r)

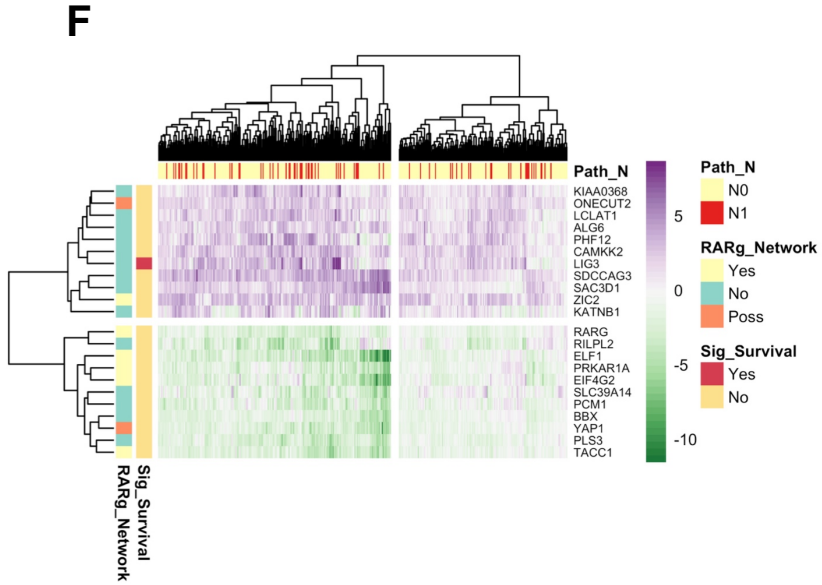
F
Path_N
KIAA0368
ONECUT2
LCLAT1
ALG6
PHF12
CAMKK2
LIG3
SDCCAG3
SAC3D1
ZIC2
KATNB1
RARG
RILPL2
ELF1
PRKAR1A
EIF4G2
SLC39A14
PCM1
BBX
YAP1
PLS3
TACC1
RARg_Network
Sig_Survival
Path_N
N0
N1
RARg_Network
Yes
No
Poss
Sig_Survival
Yes
No

Figure 5

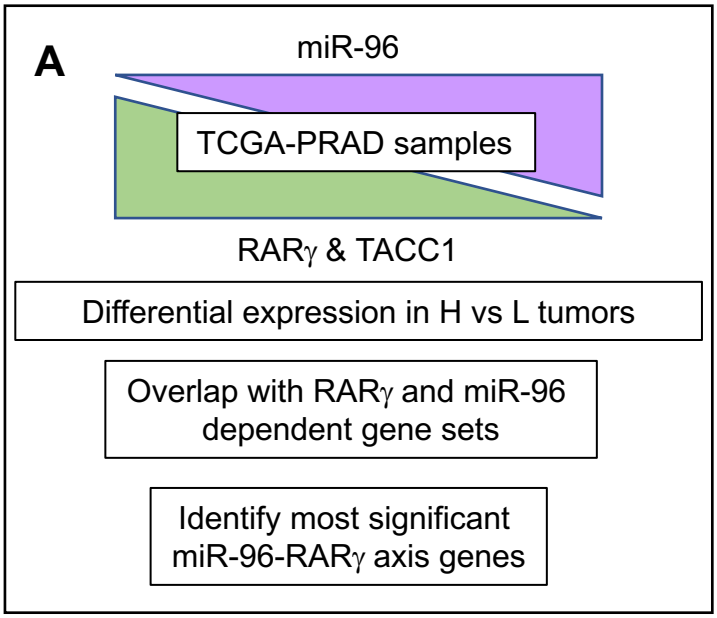
A
miR-96
TCGA-PRAD samples
RARγ & TACC1
Differential expression in H vs L tumors
Overlap with RARγ and miR-96 dependent gene sets
Identify most significant miR-96-RARγ axis genes

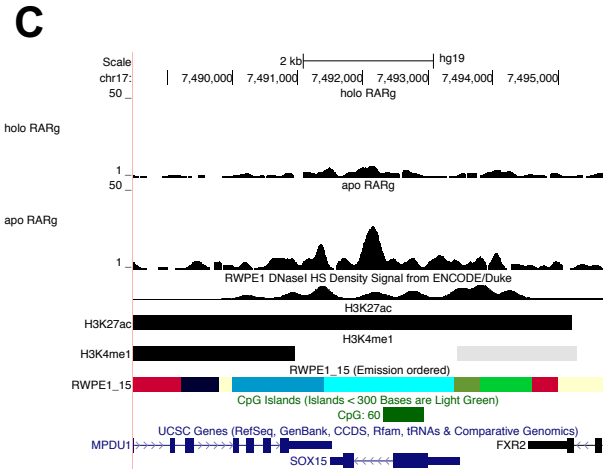
C
Scale
chr17:
2 kb
hg19
7,490,000
7,491,000
7,492,000
7,493,000
7,494,000
7,495,000
holo RARg
apo RARg
RWPE1 DNaseI HS Density Signal from ENCODE/Duke
H3K27ac
H3K4me1
RWPE1_15 (Emission ordered)
RWPE1_15
CpG Islands (Islands < 300 Bases are Light Green)
CpG: 60
UCSC Genes (RefSeq, GenBank, CCDS, Rfam, tRNAs & Comparative Genomics)
MPDU1
SOX15
FXR2

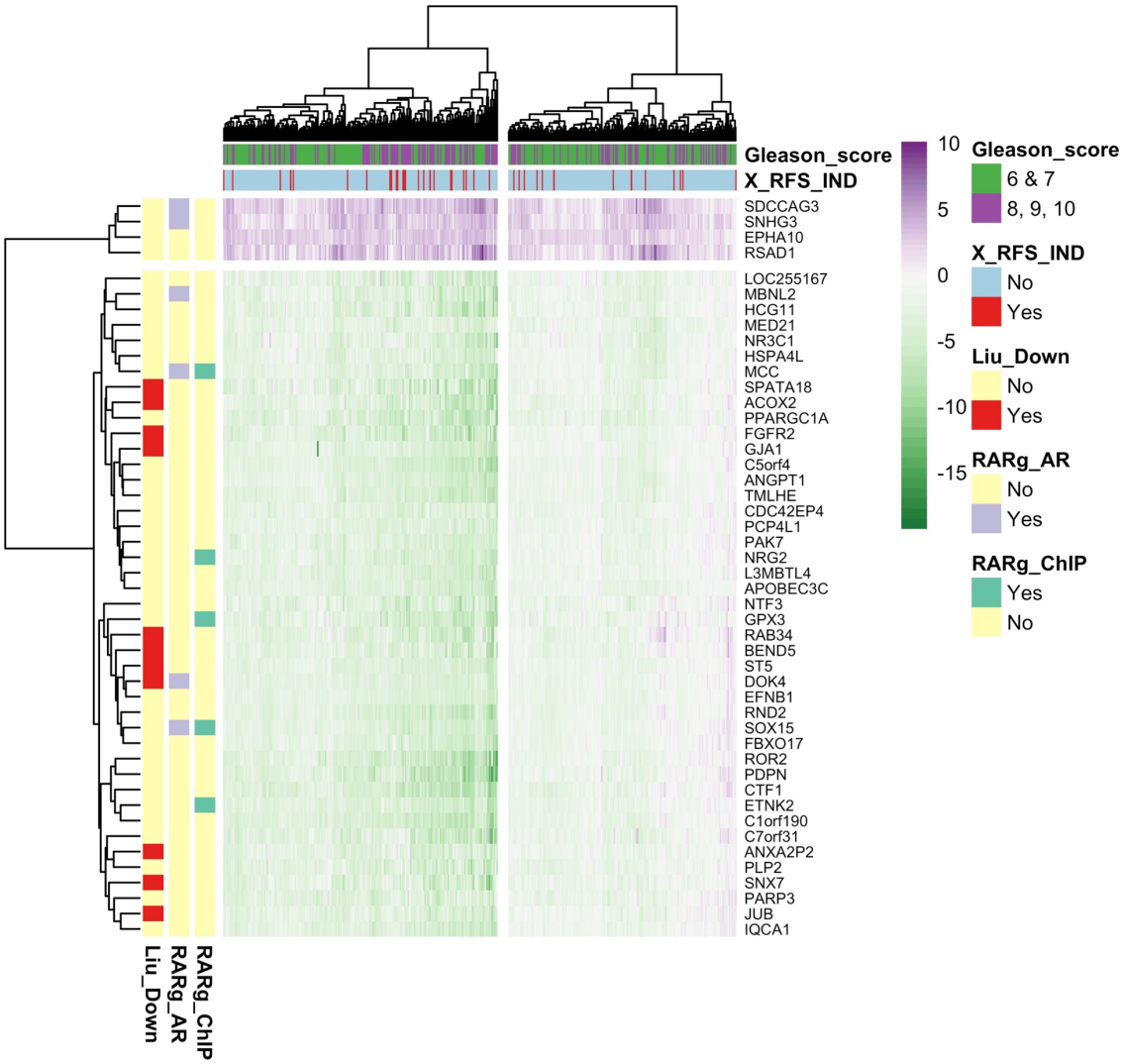
B
Gleason_score
X_RFS_IND
SDCCAG3
SNHG3
EPHA10
RSAD1
LOC255167
MBNL2
HCG11
MED21
NR3C1
HSPA4L
MCC
SPATA18
ACOX2
PPARGC1A
FGFR2
GJA1
C5orf4
ANGPT1
TMLHE
CDC42EP4
PCP4L1
PAK7
NRG2
L3MBTL4
APOBEC3C
NTF3
GPX3
RAB34
BEND5
ST5
DOK4
EFNB1
RND2
SOX15
FBXO17
ROR2
PDPN
CTF1
ETNK2
C1orf190
C7orf31
ANXA2P2
PLP2
SNX7
PARP3
JUB
IQCA1
Liu_Down
RARg_AR
RARg_ChIP
10
5
0
-5
-10
-15
Gleason_score
6 & 7
8, 9, 10
X_RFS_IND
No
Yes
Liu_Down
No
Yes
RARg_AR
No
Yes
RARg_ChIP
Yes
No